

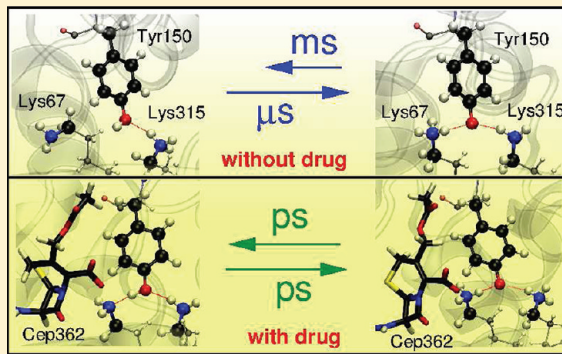
# Thermodynamic and Kinetic Stabilities of Active Site Protonation States of Class C $\beta$ -Lactamase

Ravi Tripathi and Nisanth N. Nair\*

Department of Chemistry, Indian Institute of Technology, Kanpur, 208016 Kanpur, India

Supporting Information

**ABSTRACT:** By employing computationally intensive molecular dynamics simulations using hybrid quantum-mechanical/molecular-mechanical approach, we analyze here the kinetic and thermodynamic stabilities of various active site protonation states of a fully solvated class C  $\beta$ -lactamase. We report the detailed mechanism of proton transfer between catalytically important active site residues and the associated free energy barriers. In the apoenzyme, significant structural changes are associated with the proton transfer, and the orientations of active site residues are distinctly different for various protonation states. Among several propositions on the protonation state of the apoprotein, we find that the one with Tyr<sub>150</sub> deprotonated and both Lys<sub>67</sub> and Lys<sub>315</sub> residues being protonated is the most stable one, both thermodynamically and kinetically. However, the equilibrium structure at room temperature is a dynamic one, with Lys<sub>315</sub>H <sub>$\zeta$</sub>  delocalized between Tyr<sub>150</sub>O <sub>$\eta$</sub>  and Lys<sub>315</sub>N <sub>$\zeta$</sub> . Of great importance, the kinetic and thermodynamic stability of protonation states are significantly affected on noncovalently complexing with cephalothin, an antibiotic molecule. The equilibrium structure of the enzyme–substrate (precovalent) complex has a dynamic protonation state where a proton shuttles frequently between the Tyr<sub>150</sub>O <sub>$\eta$</sub>  and Lys<sub>67</sub>N <sub>$\zeta$</sub> . We examine here the genesis of the manifold change in stability at the molecular level. The importance of our observations toward understanding the reactivity of the enzyme is discussed and experimental observations are rationalized.



## 1. INTRODUCTION

$\beta$ -Lactamases are bacterial enzymes that defend the activity of  $\beta$ -lactam antibiotics by cleaving the amide bond within the  $\beta$ -lactam ring of the drug molecule and consequently turning them biologically inert. Antibiotic resistance developed through this defensive mechanism is globally escalated to many pathogenic bacteria, undoubtedly, raising a serious concern for public health.<sup>1–7</sup> Contemporary antibiotics include molecules such as penems that can arrest the activity of  $\beta$ -lactamases by covalently binding to their active sites. However, the usage of these drugs could not accomplish an end to the “chemical warfare”<sup>7</sup> with bacteria, and resistance has been even developed toward several new generation antibiotics. Thus, today, we have an urgency for novel drugs that can combat the growing bacterial resistance. Molecular level understanding of interactions and reactions of antibiotic drug molecules with active site of  $\beta$ -lactamases is paramount in tailoring their specificity as well as efficiency.<sup>8</sup>

Considerable activities have taken place in this field of research: several X-ray crystallographic data and mutation and kinetics studies are available on various types of  $\beta$ -lactamases, shedding light on the protein structure, based on which numerous reaction mechanisms for the enzymatic activity have been proposed.<sup>9–17</sup> Lucid reviews on structure and reactivity of  $\beta$ -lactamases are available<sup>4,5,8,18–23</sup> and are not detailed here. Among the various classes of  $\beta$ -lactamases, the extended types

belonging to the class C superfamily<sup>24</sup> are globally distributed, causing resistance to a variety of  $\beta$ -lactam antibiotics like ampicillin and cephemycins. They are found to be even capable of devaluating the third-generation cephalosporins and carbapenems.<sup>2,25</sup> Because of their increasing clinical relevance, a large number of works has been focused on the structure and reactivity of class C  $\beta$ -lactamases.<sup>26–32</sup> The main part of the active site is a serine residue, Ser<sub>64</sub>, together with Lys<sub>67</sub>, Tyr<sub>150</sub>, Lys<sub>315</sub>, Glu<sub>272</sub>, Gln<sub>120</sub>, Asn<sub>152</sub>, His<sub>314</sub>, Thr<sub>316</sub>, and Ser<sub>318</sub>.<sup>12,13,16,33–35</sup>

The acylation and deacylation steps involved in the hydrolysis reaction<sup>36,37</sup> involve several proton transfer steps (see Figure 1). In the acylation step, Ser<sub>64</sub> attacks the carbon atom of the  $\beta$ -lactam ring, forming a covalent bond. Here a base is required to abstract the proton of Ser<sub>64</sub>O <sub>$\gamma$</sub> . It is also believed that activation of the deacylating water proceeds with the aid of a general base. Essentially, Tyr<sub>150</sub> or Lys<sub>67</sub> are proposed to act as the base.<sup>11–14,33</sup> Since these reactions involve proton transfer steps, the protonation states of the active site residues, in particular, Tyr<sub>150</sub>, Lys<sub>67</sub>, and Lys<sub>315</sub>, are decisive in the reactivity of the enzyme.<sup>38</sup> In fact, identification of protonation states of

Received: December 17, 2011

Revised: April 5, 2012

Published: April 5, 2012

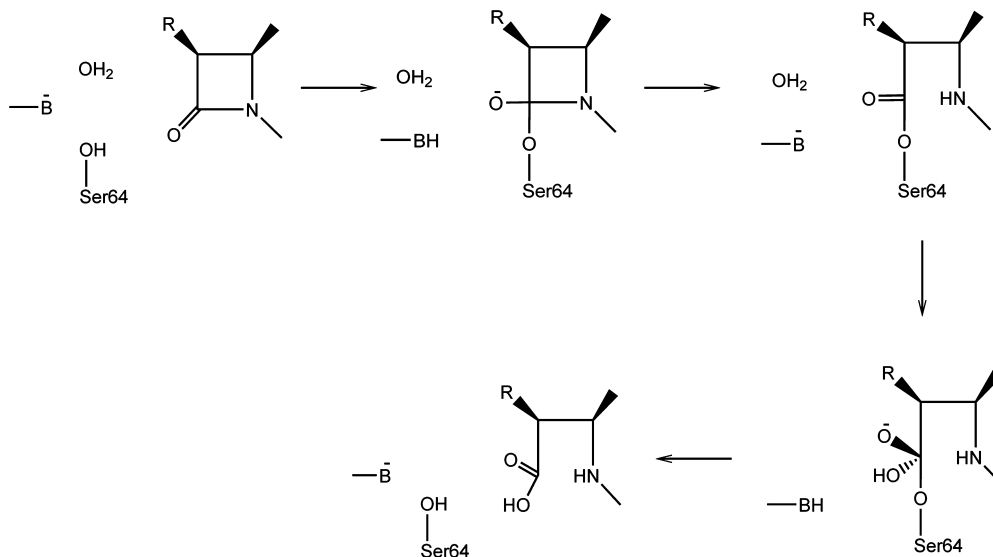


**Figure 1.** Mechanism suggested for the reaction of class C  $\beta$ -lactamase with a  $\beta$ -lactam ring of an antibiotic molecule. Series of reactions in the first row of this picture is the acylation process, and those at the bottom is the deacylation process. The general base involved in the reaction is denoted by  $B^-$ .

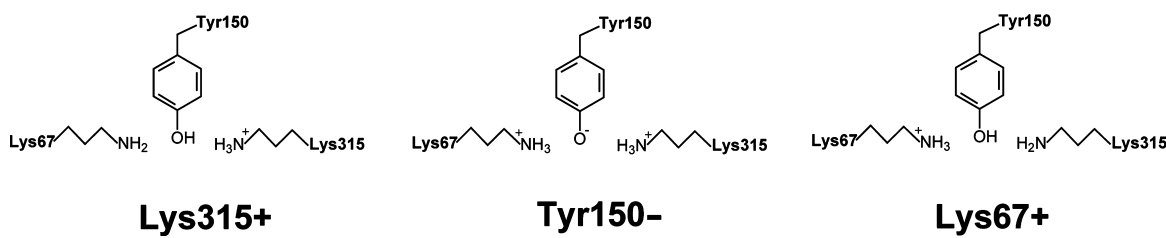


**Figure 2.** Various protonation states of  $Tyr_{150}$ ,  $Lys_{67}$ , and  $Lys_{315}$  residues in the active site of class C  $\beta$ -lactamase.

these residues could provide insight into the molecular details of the reaction mechanism.

If  $Tyr_{150}$  acts as a base to activate the catalytic center  $Ser_{64}$ , then it has to be in an anionic phenolate form. Winkler and co-workers,<sup>36</sup> on superimposing native class C enzymes to trypsin, found that  $Tyr_{150}$  is almost in the same position as histidine in trypsin and suggested  $Tyr_{150}$  in its anionic form as the general base during acylation, similar to  $His_{57}$  in trypsin.  $pK_a$  estimations using the Poisson–Boltzmann method indicated that  $Tyr_{150}$  is more likely to be in its phenolate form or in a partly protonated form, but with sufficient negative charge on  $Tyr_{150}O^-$ , and activates  $Ser_{64}$ .<sup>39</sup> Several other studies<sup>14,40,41</sup> too have highlighted the presence of the deprotonated form of  $Tyr_{150}$  and believed it to be the general base for the acylation reaction. On the other hand, a model where  $Lys_{67}$  acts as a base was developed by Dubus et al.<sup>16</sup> In their postulated reaction mechanism,  $Tyr_{150}$  does not play any important role during acylation, whereas  $Lys_{67}$  in its neutral form abstracts a proton from  $Ser_{64}O^-$ . Evidence on the existence of neutral  $Tyr_{150}$  was reported by Ishiguro et al.<sup>42</sup> on the basis of  $pK_a$  measurements using NMR spectroscopy. Moreover, study on the structure of AmpC  $\beta$ -lactamase complexed with  $\beta$ -lactam cephalothen revealed that  $Tyr_{150}$  makes hydrogen bonds with the carboxylate groups present in  $\beta$ -lactam inhibitors, favoring the existence of a protonated  $Tyr_{150}$  entity in free enzymes.<sup>37</sup> The reported high resolution crystal structure of deacylation–transition state analog of AmpC  $\beta$ -lactamase complexed with boronic acid renders that  $Tyr_{150}$  is protonated throughout the deacylation reaction.<sup>43</sup> Alternatively, a conjugate base hypoth-

esis of the reaction mechanism proposes neutral forms of both  $Tyr_{150}$  and  $Lys_{67}$ , and suggests a cooperative proton transfer between these residues during the reaction.<sup>11</sup> Along this line, some other mechanisms were also proposed in which the substrate functional group abstracts a proton either directly from  $Ser_{64}$ <sup>44,45</sup> or activate  $Tyr_{150}$  to abstract a proton from  $Ser_{64}$ .<sup>37</sup>

If we consider that  $Ser_{64}$  activation happens via a non-substrate-assisted pathway, i.e., one of the protein residue or residues in conjunction act as a base, the three residues  $Tyr_{150}$ ,  $Lys_{67}$ , and  $Lys_{315}$  that are neighboring  $Ser_{64}$  may preferably take the role of a general base. In order to trigger the proton transfer from  $Ser_{64}$ , these residues have to be in one of the three protonation states shown in Figure 2:<sup>46</sup> (a)  $Tyr_{150}$  protonated,  $Lys_{67}$  neutral, and  $Lys_{315}$  protonated; (b)  $Tyr_{150}$  deprotonated,  $Lys_{67}$  protonated, and  $Lys_{315}$  protonated, or (c)  $Tyr_{150}$  protonated,  $Lys_{67}$  protonated, and  $Lys_{315}$  neutral. These three protonation states are depicted in Figure 2 and will be identified hereafter as **Lys315+**, **Tyr150-**, and **Lys67+**, respectively.

The stability of these different protonation states in the apoprotein itself is important to understand the enzymatic action of  $\beta$ -lactamase. The detection of protonation states and determination of local  $pK_a$  values are still challenging.<sup>47,48</sup> Theoretical methods can aid in determining free energy differences between various protonation states, although simulation of the solvated protein require non-trivial modeling strategies. Average free energy differences at the semi-empirical level calculated for a series of active site structures obtained

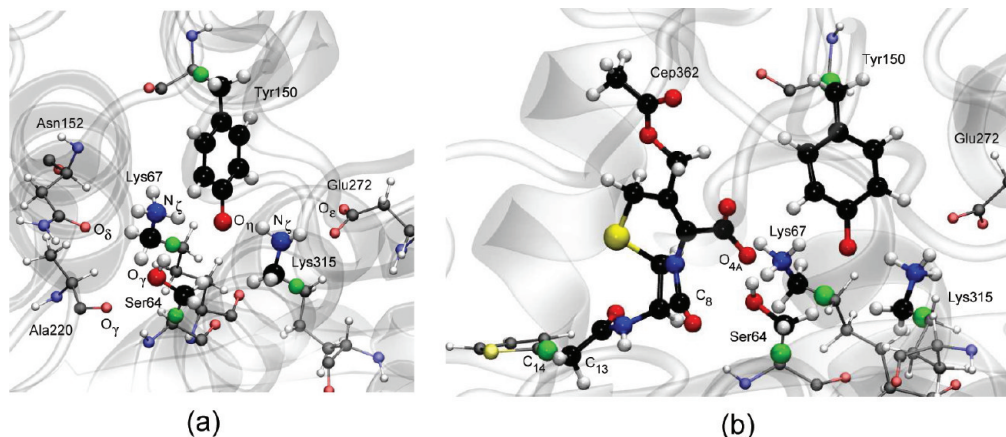


**Figure 3.** QM fragment of the protein together with the some crucial active side residues for (a) the apoenzyme and (b) the cephalothin–enzyme complex are shown using the CPK style. Residues treated quantum mechanically are highlighted with glossy spheres. Color code: C (black), O (red), N (blue), S (yellow), H (white), and capping H (green).

using classical molecular dynamics (MD) of the solvated enzyme suggested that **Tyr150-** is favored more than the other two protonation states for the apoprotein, but **Lys315+** becomes more stabilized after complexing with aztreonam.<sup>49</sup> Employing a static quantum mechanical/molecular mechanical (QM/MM) approach, Gherman et al.<sup>46</sup> reported that in a class C  $\beta$ -lactamase covalently complexed with cephalothin drug the **Tyr150-** configuration is more favored over others, although the energy difference to **Lys315+** was not appreciable (8 kJ/mol). Using a quantum mechanical treatment of the active site model of the acyl–enzyme intermediate, Hata et al.<sup>38</sup> too have predicted the same.

On the other hand, advanced modeling approaches are required to access the free energy differences including the finite temperature effects and to sample the dynamic equilibrium existing between various protonation states within a fully solvated protein environment. For systems such as  $\beta$ -lactamases, it is cardinal to go beyond the harmonic approximation in estimating the entropic contributions to the free energies due to the presence of flexible active site residues like Lys and Tyr, and their direct interactions with water molecules. Proton transfer within the active site involves bond–breaking/formation and changes in polarization of the charge density and thus simulation of such reactions requires suitable quantum mechanical treatment such as using the density functional theory (DFT). Therefore, going beyond the previous theoretical works done on class C  $\beta$ -lactamases, we employ here a computationally intensive QM/MM molecular dynamic (MD) approach where the Car–Parrinello MD method<sup>50</sup> is combined with AMBER empirical force field<sup>51</sup> based MD. Employing this technique, we investigated the protonation states and proton transfer dynamics in the active site of fully solvated *Enterobacter cloacae* 908R  $\beta$ -lactamase<sup>52</sup> and wild-type AmpC  $\beta$ -lactamase noncovalently complexed with cephalothin drug molecule.<sup>53</sup> By virtue of the metadynamics method,<sup>54,55</sup> we delineate reaction pathways connecting various protonation states and obtain associated free energy differences and free energy barriers. Thus, we scrutinize the stability of the protonation states and obtain molecular level details of the mechanism of the proton transfer processes.

## 2. METHODS AND MODELS

**2.1. System Setup and Empirical Force Field Simulation.** The structural model for the apoenzyme was constructed based on the X-ray structure of the *Enterobacter cloacae* 908R  $\beta$ -lactamase (PDB ID: 1Y54) at 2.1 Å resolution.<sup>52</sup> The coordinated penem was dissected from this complex to build up the model. Missing residues ( $\text{Thr}_1\text{-Pro}_2$ ) in the X-ray structure were added using the Modeller software.<sup>56</sup> Three different initial structures of the protein were constructed with all of the residues set to their standard protonation states, except for **Tyr150**, **Lys67**, and **Lys315**, whose protonation states were set according to the structures **Tyr150-**, **Lys315+**, and **Lys67+** (Figure 2). Each of these structures were solvated in a periodic box of dimensions  $83 \times 81 \times 90$  Å<sup>3</sup> with 14750 TIP3P water molecules. Although, the total charge of the protein is zero, we have added 2 Na<sup>+</sup> and 2 Cl<sup>-</sup> ions into the system. This was followed by energy minimization, *NPT*, and *NVT* ensemble simulations for the solvated protein in each of the protonation states (i.e., **Tyr150-**, **Lys315+**, and **Lys67+**), independently. Simulations used empirical parm99 version of AMBER force field<sup>57</sup> as implemented in the AMBER suite of programs.<sup>51</sup> While modeling the **Tyr150-** structure, we replaced the point charges of the force field for the **Tyr150** residue with the RESP charges of anionic **Tyr150** computed using the RED interface package<sup>58</sup> for a Nme–Tyr–Ace peptide model. A time step of 1 fs was used, and the nonbonded interaction cutoff was set to 15.0 Å throughout the simulation. A total of 420, 480, and 420 ps of *NPT* simulation was performed for **Lys315+**, **Tyr150-**, and **Lys67+** configurations, respectively, using Langevin thermostat set at  $T = 300$  K and barostat at  $P = 1$  atm. The subsequent *NVT* simulation was carried out for a time scale of 5 ns at the equilibrated cell volume in each case.

To analyze the effect of an antibiotic molecule on the stability of active site protonation states, we made a solvated noncovalently complexed drug–substrate model from the crystal structure of the wild-type AmpC  $\beta$ -lactamase complexed with cephalothin drug molecule (PDB ID: 1KVL).<sup>53</sup> Gly<sub>64</sub> is mutated back to Ser<sub>64</sub>, and the two protonation states **Tyr150-** and **Lys315+** of the active site were prepared. The AMBER force field was used for the protein, and the GAFF force field<sup>59</sup> was employed together with the RESP point charges (computed using RED package) to describe the cephalothin

drug molecule. The converged box of size after the *NPT* simulation (for both the protonation states) was  $79 \times 77 \times 76 \text{ \AA}^3$  with 13599 TIP3P water molecules and was used in the subsequent *NVT* and QM/MM calculations. All other technical details of the simulation are the same as that for the apoenzyme, as described in the previous paragraph.

**2.2. Hybrid QM/MM Simulation.** From the equilibrated classical simulation of Tyr150- and Lys315+ protonation states, we have performed two independent hybrid QM/MM metadynamics simulations using the CPMD/GROMOS interface, as available in the CPMD program package.<sup>60</sup> QM/MM simulations were not carried out for the Lys67+ structure, because this protonation state is ruled out after analyzing the classical force–field simulation results, as described in section 3.1. QM part of the protein encompassed the side chains of Ser<sub>64</sub>, Lys<sub>67</sub>, Tyr<sub>150</sub>, and Lys<sub>315</sub>, as shown in Figure 3, and contained a total of 33 atoms. In the QM/MM simulations using the Lys315+ structure, we included the solvent water molecule that is hydrogen–bonded to the Tyr<sub>150</sub>O<sub>η</sub> into the QM part. The QM–MM boundary was set between C<sub>α</sub>–C<sub>β</sub> and C<sub>δ</sub>–C<sub>ε</sub> bonds of QM residues, as shown in Figure 3. The dangling bonds of the C<sub>β</sub> and C<sub>ε</sub> atoms in the QM part were saturated by (capping) H atoms. Capping H atoms were constrained along the C<sub>α</sub>–C<sub>β</sub> and C<sub>δ</sub>–C<sub>ε</sub> bonds throughout the dynamics. Finite cluster boundary condition<sup>61</sup> was employed to obtain an isolated charge density of the QM part within a quantum box of size  $18 \times 16 \times 18 \text{ \AA}^3$ .

In the case of the enzyme–cephalothin complex, in addition to the side chains of Ser<sub>64</sub>, Lys<sub>67</sub>, Tyr<sub>150</sub>, and Lys<sub>315</sub>, we treated the entire drug molecule, except the thiophene ring, quantum mechanically. The capping between the thiophene residue and the rest of the cephalothin molecule was made along the Cep<sub>362</sub>C<sub>14</sub>–Cep<sub>362</sub>C<sub>13</sub>, as indicated in Figure 3b. The QM supercell used in this case was  $18 \times 21 \times 22 \text{ \AA}^3$ , having a total of 66 QM atoms.

The QM/MM coupling scheme was followed from ref 62; MM point charges that falls within 15 Å from the QM fragment were interacting with the charge density of the QM part, whereas the rest of the MM atoms interacted with a multipole expansion (up to quadrupole) of the charge density. The QM part of the protein was described using the periodic Kohn–Sham density functional theory with plane wave basis set having a planewave cutoff of 30 Ry. The PBE<sup>63</sup> exchange–correlation functional was chosen and core–electrons of all the QM atoms were described by ultrasoft pseudopotentials.<sup>64</sup>

Molecular dynamics (MD) of the QM fragment was using the Car–Parrinello method<sup>65</sup> with separate set of Nosé–Hoover chain thermostats<sup>66</sup> thermostatted to 300 K, each for the QM part, the rest of the protein, and the solvent. Integration time step of 0.145 fs was used together with a fictitious electronic orbital mass of 700 amu.

**2.3. Metadynamics Simulation.** The time scale at which a chemical reaction occurs exponentially depends on the free energy barrier that has to be surmounted. If the proton transfer process Lys315+ ⇌ Tyr150- involves substantial free energy barriers, then the time scale of the trajectories that need to be simulated by molecular dynamics becomes impractically large. For example, to observe an event that proceeds by crossing a barrier of 20 kJ/mol (or 8 k<sub>B</sub>T) at 300 K, simulation has to be performed for a few nanoseconds. Unfortunately, the time scale that can be accessed in QM/MM molecular dynamics simulations is only limited to a few tens of picoseconds. To accelerate “rare events” in computer simulations, we employed

here the metadynamics technique.<sup>54,55,67,68</sup> Exploiting this technique, we can accelerate the exploration of the system on a free energy landscape, represented using a selected set of collective coordinates. This is achieved by slowly growing repulsive potentials along the trajectory of auxiliary variables which, in turn, is strongly coupled to the collective coordinates. Of great importance is the fact that the underlying free energy surface can be mapped out using the negative sum of the added biasing potentials. This enables us to trace minimum energy pathways (MEP) connecting various minima and, thus, the molecular details of the mechanism. Moreover, we can compute free energy barriers and free energy differences along the MEP. Since the system is taken through the MEP, the technique has the power to sample unforeseen minima and often help us to go beyond our chemical intuitions.

The choice of collective coordinates, however, is crucial for the successful application of this method. Collective coordinates must incorporate motions along all “slow” degrees of freedom that are directly or indirectly involved in the reaction. Missing relevant coordinates as part of collective coordinates could slow the sampling, resulting in overestimation of the depth of the well and, thus, the free energy barriers. Details of collective coordinates used in this work will be discussed in the next section where we will present the results of metadynamics simulation. Types of collective coordinates that we used are bond distances, torsional angles, and coordination numbers. All of the technical details of the metadynamics simulation are identical to ref 69 and are not detailed here. Biasing potentials were spherical Gaussian functions with their width fixed at 0.05 and their height varied between 1 and 2 k<sub>B</sub>T depending on the extent of the reaction. Biasing potentials were updated only if the mean displacement of auxiliary variables was greater than 0.075 from the center of the previously added Gaussian.<sup>70,71</sup> Temperature of the auxiliary variables was kept close to that of the nuclear system by a direct velocity scaling whenever the temperature goes beyond the temperature window  $\pm 200$  K.

**2.4. Accuracy.** Here we briefly discuss about the accuracy of our free energy estimates. One of the main sources of error is the employed PBE density functional. This functional is known to describe the hydrogen bond interactions<sup>72</sup> well and has been used in studying the proton transfer process in enzymes using the QM/MM method.<sup>73–75</sup>

Hybrid functionals like mPW1K<sup>76,77</sup> that are known to reproduce free energy barriers and free energy differences accurately are computationally unaffordable in performing molecular dynamics simulation, especially with its planewave basis set implementation. In order to estimate the error due to the PBE functional for our system, we evaluated the energy barrier for Tyr150- → Lys315+ process using various (hybrid and meta-GGA) density functionals in static gasphase quantum mechanical calculations. All of the calculations were carried out using the Gaussian 09<sup>78</sup> suite of programs with the 6-31G+\*\* basis set using PBE, mPW1K, B3LYP,<sup>79,80</sup> and M06<sup>81</sup> density functionals. In each case, the minimum and the transition state structures of the QM residues were used to benchmark the performance of the PBE functional. It is clear from Table 1 that the potential energy barrier computed using PBE functional is in good agreement with the other meta-GGA and hybrid density functionals. This data indicates that the maximum error in the free energy estimate is about 4 kJ/mol (wrt mPW1K). This is less than the error estimate of DFT/PBE with reference to MP2/aug-cc-pVTZ as reported in ref 82.

**Table 1.** Potential Energy Barrier  $\Delta E^\ddagger$  (kJ/mol) Going from  $\text{Tyr150}^- \rightarrow \text{Lys315}^+$  in Vacuo Using Various Density Functionals

functional	$\Delta E^\ddagger$ (kJ/mol)
PBE	50
B3LYP	50
M06	52
mPW1K	54

Metadynamics technique has been successfully used for elucidating proton transfer processes; see refs 68, 69, 75, and 83–87 to name a few. Error in the free energies introduced by the metadynamics can be estimated<sup>88</sup> and is of the order of  $\pm 2k_B T \approx \pm 5$  kJ/mol for the current simulation setup. However, the error due to a missing collective coordinate is not accountable and results in overestimation of free energy barriers. A more accurate estimate of free energies can be done using post-metadynamics simulation procedures employing transition path sampling<sup>89,90</sup> and umbrella sampling along the minimum energy pathway;<sup>70</sup> however, they are not used in this work. Thus the free energy barriers obtained by the current simulation protocol are only used for a qualitative understanding of structure of the active site and the mechanism of proton transfer. The properties that are more sensitive to the free energy estimate, like reaction rates and  $pK_a$  values, are therefore not computed here.

### 3. RESULTS

**3.1. Analysis Empirical Force Field MD Simulation of the Apoenzyme.** As the first step, we performed three independent empirical force field MD simulations for the solvated protein in  $\text{Lys315}^+$ ,  $\text{Tyr150}^-$ , and  $\text{Lys67}^+$  configurations, which mutually differ in the protonation states of some active site residues (see Figure 2). Root mean square deviations (rmsd) of the protein backbone measured in all three simulations are less than 1.6 Å with respect to the first frame of the NVT simulation (see also FigSI 1), reflecting that the protein structure was stable throughout 5 ns of the NVT simulation. For the  $\text{Lys315}^+$  structure, we observed two minimum structures, as pointed out in the rmsd plots of the active site in Figure 4. One is a short-lived structure, observed in the initial stages of the simulation, hereafter noted as  $\text{Lys315A}^+$ ; see Figure 5b and Table 2 for their structural differences. The long-lived  $\text{Lys315}^+$  structure is much closer to the X-ray structure than  $\text{Lys315A}^+$  (Table 2); the active site rmsd of  $\text{Lys315}^+$  is about 1.47 Å in average with reference to the crystal structure. Only one minimum structure was observed in the simulation of  $\text{Tyr150}^-$ . rmsd of the active site of this structure with respect to the X-ray structure is only 1.25 Å. Moreover, the structural parameters of this structure resemble well to the crystal structure (Table 2). Large deviation from the X-ray structure was observed for the equilibrium structure of the  $\text{Lys67}^+$  protonation state (Figure 5d); see Table 2. rmsd of the active site is 1.82 Å in average with respect to the crystal structure. For a metastable structure,  $\text{Lys67A}^+$ , observed during the same simulation has an rmsd of only 1.21 Å relative to the crystal structure. Interestingly, its active site structure resembles well with the deprotonated  $\text{Lys}_{315}$  state reported by Diaz et al.<sup>49</sup> The so-called “oxyanion hole”<sup>91–93</sup> consisting  $\text{Ser}_{64}\text{NH}$  and  $\text{Ser}_{318}\text{NH}$ , which is believed to be crucial in stabilizing the acyl–enzyme tetrahedral intermediate

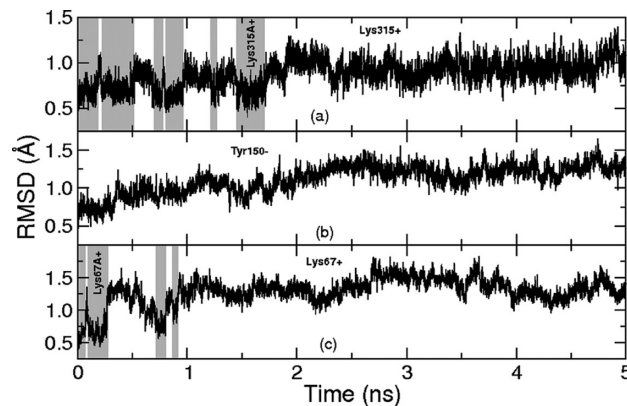


**Figure 4.** rmsd of the active site with respect to the starting structure of the NVT simulation during the empirical force field based MD simulation for (a)  $\text{Lys315}^+$ , (b)  $\text{Tyr150}^-$ , and (c)  $\text{Lys67}^+$  protonation states. Shaded regions show the occurrences of intermediates  $\text{Lys315A}^+$  and  $\text{Lys67A}^+$  in (a) and (b), respectively. See Figure 5 for structures corresponding to these nomenclatures.

during the acylation reactions in serine  $\beta$ -lactamases was stable in all of the simulations.

$\text{Tyr}_{150}$  phenyl  $\text{Tyr}_{112}$  phenyl ring interaction is intact in  $\text{Lys315}^+$  as well as in  $\text{Tyr150}^-$  case, whereas it is completely lost in  $\text{Lys67}^+$ . The proximity of  $\text{Tyr}_{150}\text{O}_\eta$  and carboxylate  $\text{Glu}_{272}\text{O}_\epsilon$  in  $\text{Lys67}^+$  is not in agreement with the crystal structure.<sup>36</sup> Further, having  $\text{Lys67}^+$  as the most stable protonation state will not be useful for the protein to functionalize efficiently, since the mechanism of acylation involves a delocalization of the proton from  $\text{Ser}_{64}$  through a basic entity, and the basic entity in the  $\text{Lys67}^+$  case, i.e., the  $\text{Lys}_{315}$  moiety, lies far from  $\text{Ser}_{64}$  to activate this residue. Therefore, the  $\text{Lys67}^+$  protonation state cannot be the stable protonation state of the active site. On the other hand, the  $\text{Lys315}^+$  structure is a crucial structure to consider since  $\text{Lys}_{67}$  is in an appropriate orientation to delocalize the proton of  $\text{Ser}_{64}$ . In the  $\text{Tyr150}^-$  structure, despite having the  $\text{Tyr}_{150}\text{O}_\eta \cdots \text{Ser}_{64}\text{H}_\gamma$  distance of 4.28 Å, two possible mechanisms of activation can be envisaged: (a) a direct proton abstraction by  $\text{Tyr}_{150}$  considering its flexibility of this residue, and (b) a proton hopping from  $\text{Lys}_{67}$  to  $\text{Tyr}_{150}$  followed by that from  $\text{Ser}_{64}$  to  $\text{Lys}_{67}$ . Based on the above arguments, the active site protonation state could be either  $\text{Lys315}^+$  or  $\text{Tyr150}^-$  but not  $\text{Lys67}^+$ . This is also in line with previous free energy calculations.<sup>38,46,49</sup> Thus we excluded the  $\text{Lys67}^+$  protonation state and had not considered it for the subsequent proton transfer simulations.

**3.2. QM/MM Canonical Ensemble Simulation of  $\text{Lys315}^+$  and  $\text{Tyr150}^-$ .** To access the stability of  $\text{Tyr150}^-$  structure, a canonical ensemble hybrid QM/MM simulation was performed initially with  $\text{Tyr150}^-$  structure. Since proton transfer process are not captured in the empirical force field based simulation, it is critical to have the QM/MM framework to simulate such events. During this 5 ps QM/MM MD simulation, we saw that hydrogen bonds  $\text{Lys}_{67}\text{H}_\zeta \cdots \text{Tyr}_{150}\text{O}_\eta$  and  $\text{Lys}_{315}\text{H}_\zeta \cdots \text{Tyr}_{150}\text{O}_\eta$  remained stable throughout (see Figure 6a). Interestingly, the  $\text{Lys}_{315}\text{H}_\zeta$  that is hydrogen bonded to the  $\text{Tyr}_{150}\text{O}_\eta$  shuttles frequently between the  $\text{Lys}_{315}\text{N}_\zeta$  and  $\text{Tyr}_{150}\text{O}_\eta$ . Snapshots from a reactive trajectory are shown in Figure 6 b-d. All other interactions in the active site remained intact during this simulation. Proton transfer from  $\text{Lys}_{315}\text{N}_\zeta$  to  $\text{Tyr}_{150}\text{O}_\eta$  resulted in structure  $\text{Lys67B}^+$  that is very similar to

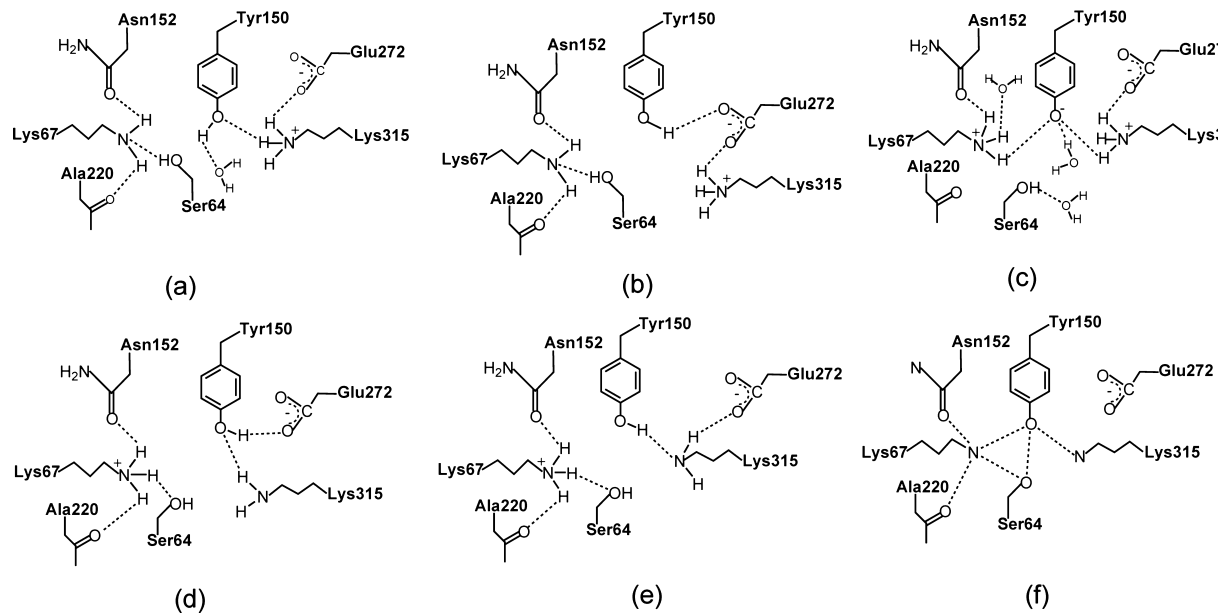


**Figure 5.** Schematic representation of the active site structure for several intermediates observed using empirical force field based MD (a–e) and X-ray crystal structure<sup>36</sup> (f). Structures are labeled as (a) Lys315+, (b) Lys315A+, (c) Tyr150-, (d) Lys67+, and (e) Lys67A+. See also FigS1 2.

**Table 2. Average Distance (in Å) between Selected Residues in the Active Site of Various Minimum Energy Structures of Class C  $\beta$ -Lactamase Computed from the Classical Molecular Dynamics Simulation, in Comparison with That of the Crystal Structure of the Apoenzyme (1FRI<sup>b</sup>, chain A), and the Crystal Structure of the Enzyme Complexed with Penem (IY54<sup>c</sup>)<sup>a</sup>**

distance	1FRI <sup>b</sup>	IY54 <sup>c</sup>	Lys315+	Lys315A+	Tyr150-	Lys67+	Lys67A+
Tyr <sub>150</sub> O <sub>η</sub> ···Lys <sub>67</sub> N <sub>ζ</sub>	3.51	3.06	4.91 (0.41)	6.07 (0.52)	2.90 (0.21)	7.76 (1.04)	4.65 (0.47)
Tyr <sub>150</sub> O <sub>η</sub> ···Lys <sub>315</sub> N <sub>ζ</sub>	2.98	2.90	3.05 (0.26)	3.60 (0.58)	2.86 (0.26)	4.6 (1.22)	3.09 (0.35)
Lys <sub>67</sub> N <sub>ζ</sub> ···Asn <sub>152</sub> O <sub>δ</sub>	2.76	2.78	2.92 (0.15)	2.90 (0.15)	4.40 (1.46)	3.44 (1.05)	2.79 (0.12)
Lys <sub>67</sub> N <sub>ζ</sub> ···Gly <sub>220</sub> O <sub>γ</sub>	2.96	2.78	3.00 (0.19)	3.03 (0.20)	5.18 (0.47)	4.06 (0.98)	2.87 (0.24)
Lys <sub>315</sub> N <sub>ζ</sub> ···Glu <sub>272</sub> O <sub>ε</sub>	4.45	4.53	3.23 (0.52)	3.48 (0.53)	2.83 (0.14)	6.07 (0.90)	3.37 (0.65)
Lys <sub>67</sub> N <sub>ζ</sub> ···Ser <sub>64</sub> O <sub>γ</sub>	2.56	3.56	2.74 (0.16)	2.76 (0.16)	3.28 (0.44)	3.77 (0.90)	2.91 (0.22)
Tyr <sub>150</sub> O <sub>η</sub> ···Ser <sub>64</sub> O <sub>γ</sub>	3.01	3.14	4.55 (0.54)	5.52 (0.45)	4.09 (0.51)	8.95 (0.87)	4.13 (0.47)

<sup>a</sup>Standard deviation measured during the trajectory is shown in brackets. <sup>b</sup>Reference 36. <sup>c</sup>Reference 52.

the Lys67A+ structure which was observed during the classical simulation, except in the alignment of Lys<sub>67</sub>. This residue is hydrogen bonded to Ser<sub>64</sub> in Lys67A+, whereas it is hydrogen bonded to Tyr<sub>150</sub> in Lys67B+. Also the average distances of Tyr<sub>150</sub>O<sub>η</sub>···Lys<sub>67</sub>N<sub>ζ</sub> in Lys67A+ and Lys67B+ structures are 4.9 and 2.5 Å, respectively. Most importantly, Lys67B+ is only a transient structure and it goes back spontaneously to the Tyr150- structure. This implies also that the forward and backward free energy barrier for Tyr150- ⇌ Lys67B+ is of the order of about 1 k<sub>B</sub>T<sub>300K</sub> (~2.5 kJ/mol). Thus at equilibrium, Tyr150- has a dynamical structure, where Lys<sub>315</sub>H<sub>ζ</sub> is partially delocalized between the Tyr<sub>150</sub>O<sub>η</sub> and Lys<sub>315</sub>N<sub>ζ</sub>. The formation of Lys67+ was not observed in the time scale of the simulation since the Lys67B+ → Lys67+ involves large displacement of the active site residues, and thus involves relatively high free energy barrier.

Independent of the above simulation, we performed 3 ps of canonical ensemble QM/MM simulation of Lys315+ structure. The structure remained without any appreciable changes throughout the simulation, and the average structure of the active site show some minor differences in the averages (and standard deviations) obtained from classical simulation of Lys315+. For example, the average distance between Lys<sub>67</sub>N<sub>ζ</sub> and Tyr<sub>150</sub>O<sub>η</sub> measured from classical and QM/MM simulations are 4.91 ( $\pm 0.2$ ) and 5.31 ( $\pm 0.41$ ) Å, respectively.

**3.3. Tyr150- → Lys315+ Proton Transfer Dynamics.** As the next step, we explored the proton transfer dynamics in going from Tyr150- to Lys315+ protonation state, employing the metadynamics technique within the QM/MM setup. We chose two collective coordinates to simulate the transformation from Tyr150- → Lys315+ in our metadynamics simulation: (a) distance between Tyr<sub>150</sub>O<sub>η</sub> and Lys<sub>67</sub>N<sub>ζ</sub>, d[O<sub>150</sub>–N<sub>67</sub>], and (b) coordination number between the Tyr<sub>150</sub>O<sub>η</sub> and three hydrogens Lys<sub>67</sub>H<sub>ζ</sub>, C[O<sub>150</sub>–H<sub>67</sub>]. The first collective coordinate was chosen for accelerating the (slow) motion of the Lys<sub>67</sub> and Tyr<sub>150</sub> with respect to each other and is critical in differentiating Lys315A+ and Lys315+ on the free energy surface. However, sampling along this distance may also drive the transformation from Tyr150- to Lys67+. To avoid this to happen, we introduced a wall potential on the collective coordinates along d[O<sub>150</sub>–N<sub>67</sub>] at 4.5 Å when C[O<sub>150</sub>–H<sub>67</sub>] < 0.2. The reconstructed free energy surface from this simulation is shown in Figure 7a. Minimum energy pathway (Figure 7b) was then traced on this three-dimensional surface to estimate the free energy differences between various configurations.

Note here that Tyr150- contains some percentage of Lys67B+ structure too, as described in the previous section. By crossing a free energy barrier of 20 kJ/mol, the Tyr150- structure converts to an ensemble of structures resembling

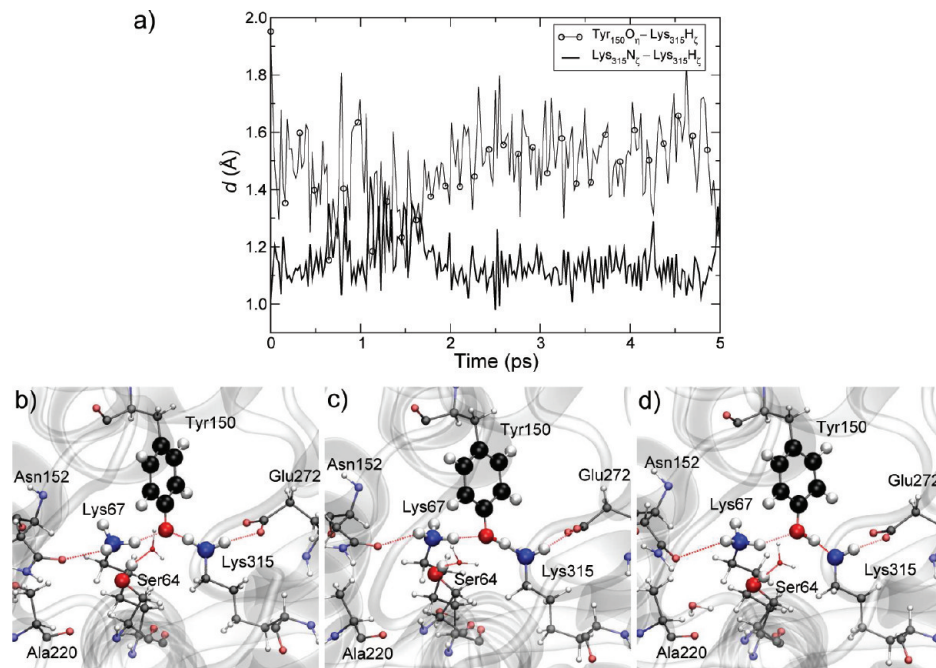


**Figure 6.** (a) Distance between  $\text{Tyr}_{150}\text{O}_\eta \cdots \text{Lys}_{315}\text{H}_\zeta$  (circle) and  $\text{Lys}_{315}\text{N}_\zeta \cdots \text{Lys}_{315}\text{H}_\zeta$  during the QM/MM canonical ensemble simulation of  $\text{Tyr}_{150}$ -protonation state. Representative snapshots of (b)  $\text{Tyr}_{150}$ -, (c) transition state structure for the proton transfer, and (d)  $\text{Lys}_{67}\text{B}^+$ .

$\text{Lys}_{67}\text{A}^+$  that are almost 10 kJ/mol higher in energy than the former.

The free energy barrier for a proton transfer to occur from  $\text{Lys}_{67}\text{N}_\zeta$  to  $\text{Tyr}_{150}\text{O}_\eta$  is about 31 kJ/mol. The resultant

structure,  $\text{Lys}_{315}\text{B}^+$ , resembles neither  $\text{Lys}_{315}^+$  nor  $\text{Lys}_{315}\text{A}^+$  due to the close contact of  $\text{Tyr}_{150}$  and  $\text{Lys}_{67}$  in  $\text{Lys}_{315}\text{B}^+$ :  $d[\text{O}_{150}-\text{N}_{67}] \approx 3 \text{ \AA}$  (see Figure 8a). The structure also has  $C[\text{O}_{150} - \text{H}_{67}] \approx 0.5$ , indicating that proton is delocalized between  $\text{Lys}_{67}$  and  $\text{Tyr}_{150}$ . The reverse barrier of 4 kJ/mol ( $\sim 1.6 k_B T_{300 \text{ K}}$ ) signifies that  $\text{Lys}_{315}\text{B}^+$  is metastable and largely goes back to  $\text{Tyr}_{150}$ - In the metadynamics trajectory proton shuttling continued between the two residues until  $d[\text{O}_{150}-\text{N}_{67}]$  increased substantially; see also Figure 8b. A complete transfer of proton and subsequent increase in  $d[\text{O}_{150}-\text{N}_{67}]$  resulted in the formation of the  $\text{Lys}_{315}^+$  structure. Nearly 67 kJ/mol more energy is required for  $\text{Lys}_{315}\text{B}^+ \rightarrow \text{Lys}_{315}^+$  conversion. Potential energy needed to break apart electrostatically bound  $\text{Tyr}_{150}\text{H}_\eta$  and  $\text{Lys}_{67}\text{N}_\zeta$  residues as well as the energy requirement for the collective structural changes involving neighboring residues may contribute substantially to this barrier. The effective free energy barrier for  $\text{Tyr}_{150}^- \rightarrow \text{Lys}_{315}^+$  is about 94 kJ/mol and thus this event occurs at a time scale of a few milliseconds. Substantial structural rearrangements occurred after crossing the transition state (Figure 8b), subsequently forming the  $\text{Lys}_{315}^+$  structure (Figure 5a).

For the estimation of the reverse barrier, i.e. going from  $\text{Lys}_{315}^+$  to  $\text{Tyr}_{150}$ -, metadynamics simulation should be continued until  $\text{Lys}_{315}^+ \rightarrow \text{Tyr}_{150}^-$  is observed. However, for complex systems like enzymes, the forward and reverse process may proceed through different pathways due to irreversible structural changes occurring at the active site. The collective coordinates that were defined for the forward process may not be sufficient to simulate the reverse process. Therefore the simulation was not continued until the product free energy well was fully sampled, and thus it is not possible to evaluate exact depth of  $\text{Lys}_{315}^+$  minimum and the free energy difference between  $\text{Lys}_{315}^+$  and  $\text{Tyr}_{150}^-$  from this simulation.

### 3.4. $\text{Lys}_{315}^+ \rightarrow \text{Tyr}_{150}^-$ Proton Transfer Dynamics.

Subsequently, we looked into  $\text{Lys}_{315}^+ \rightarrow \text{Tyr}_{150}^-$  in order to simulate the reverse process, and thus to obtain kinetic and

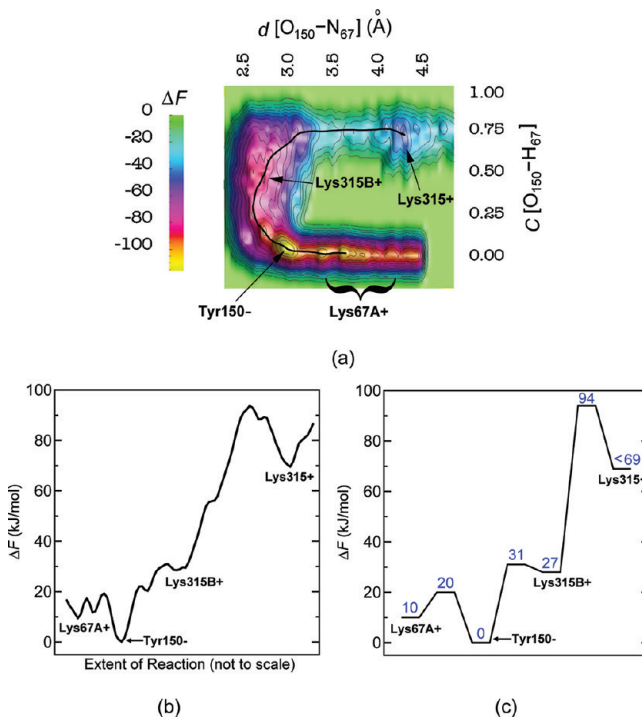


**Figure 7.** (a) Reconstructed free energy surface for the conversion of  $\text{Tyr}_{150}^-$  to  $\text{Lys}_{315}^+$ . Free energies are in kJ/mol. Minimum energy structures are labeled on the surface. The traced minimum energy pathway is shown as a black curve. (b) Free energy change along the minimum energy pathway traced on the free energy surface. (c) Free energy profile for the process.

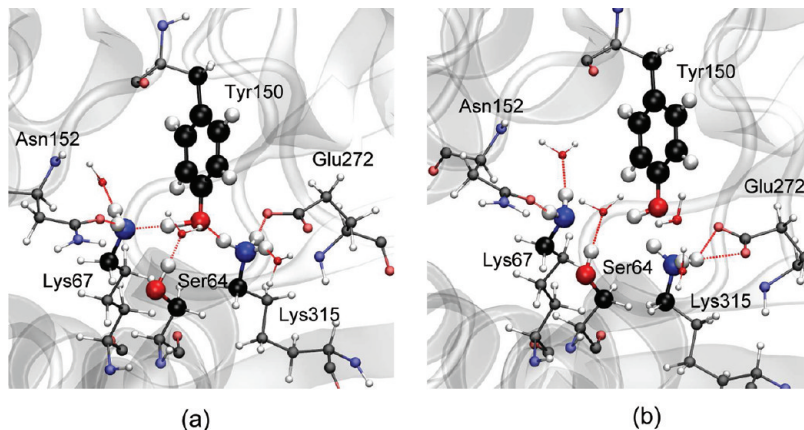


**Figure 8.** (a) Observed intermediate  $\text{Lys315B}^+$  and (b) the transition state structure observed during the metadynamics simulation of  $\text{Tyr150}^- \rightarrow \text{Lys315}^+$ .

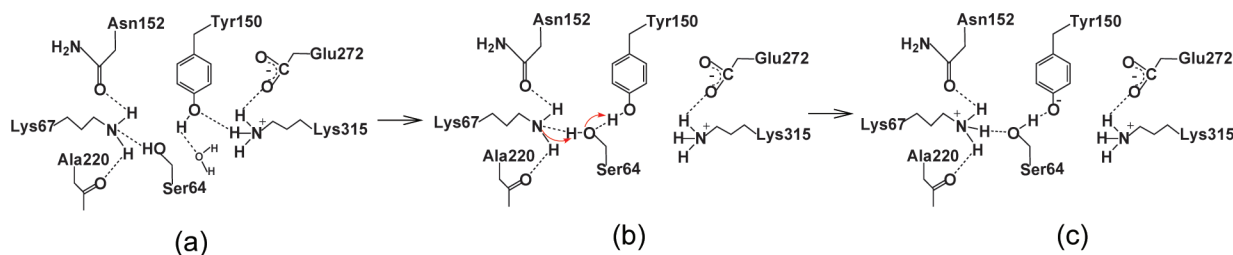


**Figure 9.** Schematic view of proton transfer from  $\text{Tyr}_{150}$  to  $\text{Lys}_{67}$  via  $\text{Ser}_{64}$  bridging.

thermodynamic stabilities of  $\text{Lys315}^+$  and  $\text{Tyr150}^-$ . We initially performed a metadynamics simulation using three collective coordinates: (a) distance between  $\text{Lys}_{67}\text{N}_\zeta$  and  $\text{Tyr}_{150}\text{O}_\eta$ ,  $d[\text{N}_{67}-\text{O}_{150}]$ ; (b) coordination number of  $\text{Lys}_{67}\text{N}_\zeta$  with  $\text{Lys}_{67}\text{H}_\zeta$  and  $\text{Tyr}_{150}\text{H}_\eta$ ,  $C[\text{N}_{67}-\text{H}_{67,150}]$ ; (c) torsional angle formed by  $\text{H}-\text{O}-\text{C}_\alpha-\text{C}_\beta$  of  $\text{Ser}_{64}$ ,  $\phi[\text{H}-\text{O}-\text{C}_\alpha-\text{C}_\beta]_{64}$ . The first coordinate was taken for bringing  $\text{Lys}_{67}$  and  $\text{Tyr}_{150}$  residues near, while the second one was meant to trigger the proton transfer from  $\text{Tyr}_{150}$  to  $\text{Lys}_{67}$ . The third coordinate was defined in accelerating the twisting along the torsional angle about  $\text{O}-\text{C}_\alpha$  bond in  $\text{Ser}_{64}$ , and thus going from a “pointing toward  $\text{Lys}_{67}$ ” to a “pointing toward water” configuration (see Figure 5).

It is well-known that TIP3P water model overestimate the dipole moments of isolated water molecules resulting in the stronger hydrogen bonds. During the process  $\text{Lys315}^+ \rightarrow \text{Tyr150}^-$ , scission of  $\text{Tyr}_{150}\text{H}_\eta \cdots \text{H}_2\text{O}$  hydrogen bond has to take place initially. In order to avoid overestimation of free energy barriers as a result of the artifact of TIP3P model, the water molecule that is hydrogen bonded to  $\text{Tyr}_{150}$  in  $\text{Lys315}^+$  structure was treated quantum mechanically.

In the metadynamics trajectory, the first sequence of events included the breakage of  $\text{Tyr}_{150}\text{H}_\eta \cdots \text{H}_2\text{O}$  hydrogen bond followed by movement of  $\text{Tyr}_{150}$  toward  $\text{Ser}_{64}$ . For several occurrences, consecutive proton transfers were observed from  $\text{Ser}_{64}$  to  $\text{Lys}_{67}$  and from  $\text{Tyr}_{150}$  to  $\text{Ser}_{64}$ . The facile movement of  $\text{Tyr}_{150}$  and a direct interaction between  $\text{Tyr}_{150}$  and  $\text{Ser}_{64}$  was unforeseen and opened up the possibility of an indirect proton transfer pathway, as depicted in Figure 9.

To verify such a pathway, we performed a fresh metadynamics simulation, with a new set of collective coordinates: (a) distance between  $\text{Ser}_{64}\text{O}_\gamma$  and  $\text{Tyr}_{150}\text{O}_\eta$ ,  $d[\text{O}_{64}-\text{O}_{150}]$ ; (b) coordination number of  $\text{Lys}_{67}\text{N}_\zeta$  with  $\text{Lys}_{67}\text{H}_\zeta$ ,  $C[\text{N}_{67}-\text{H}_{67}]$ . In the structure  $\text{Tyr150A}^-$ , the coordinate  $C[\text{H}_{64}-\text{O}_{150}] \approx 0$ . Since a proton transfer from

$\text{Lys}_{67}\text{H}_\zeta$ ,  $\text{Ser}_{64}\text{H}_\gamma$  and  $\text{Tyr}_{150}\text{H}_\eta$ ,  $C[\text{N}_{67}-\text{H}_{67,150}]$ ; (c) coordination number of  $\text{Ser}_{64}\text{O}_\gamma$  and  $\text{Tyr}_{150}\text{H}_\eta$ ,  $C[\text{O}_{64}-\text{H}_{150}]$ . The first coordinate was defined for sampling the motion of  $\text{Tyr}_{150}$  toward  $\text{Ser}_{64}$ . To accelerate proton transfer from  $\text{Lys}_{67}$ , either directly to  $\text{Tyr}_{150}$ , or from  $\text{Ser}_{64}$  as in the mechanism in Figure 9, we used the coordinate  $C[\text{N}_{67}-\text{H}_{64,67,150}]$ . The proton transfer between  $\text{Tyr}_{150}$  and  $\text{Ser}_{64}$  was sampled by the third coordinate.

The reconstructed free energy surface is available in FigSI 3 and the free energy profile is shown in Figure 10a. At first, we observed an intermediate  $\text{Lys315C}^+$ , which resembles in all its structural features  $\text{Lys315}^+$ , but the distance between  $\text{Ser}_{64}$  and  $\text{Tyr}_{150}$  residue (Figure 10b). This structure was sampled after crossing a free energy barrier of 28 kJ/mol, and the reverse barrier is approximately 20 kJ/mol. The intermediate  $\text{Lys315C}^+$  further crossed a barrier of about 25 kJ/mol to another minimum  $\text{Lys315D}^+$  where  $\text{Tyr}_{150}$  comes more closer to  $\text{Ser}_{64}$  compared to  $\text{Lys315C}^+$ , and forms a hydrogen bond with the latter (Figure 10c).  $\text{Lys315D}^+$  undergoes proton transfer from  $\text{Ser}_{64}$  to  $\text{Lys}_{67}$ , followed by  $\text{Tyr}_{150}$  to  $\text{Ser}_{64}$ , surmounting a relatively small free energy barrier of about 12 kJ/mol, forming a configuration as in Figure 10d. This structure,  $\text{Tyr150A}^-$ , differs from  $\text{Tyr150}^-$  in the positions of  $\text{Tyr}_{150}$  and  $\text{Lys}_{67}$ .

On analysis, we realized that conversion from  $\text{Tyr150A}^-$  to  $\text{Tyr150}^-$  involves several rearrangements of the active side residues, as well as breakage of several hydrogen bonds. Thus to simulate this conversion, we performed two more metadynamics simulations in sequence. In the first one, we used three collective coordinates: (a) coordination number of  $\text{Ser}_{64}\text{H}_\gamma$  and  $\text{Tyr}_{150}\text{O}_\eta$ ,  $C[\text{H}_{64}-\text{O}_{150}]$ ; (b) distance between  $\text{Ser}_{64}\text{O}_\gamma$  and  $\text{Tyr}_{150}\text{O}_\eta$ ,  $d[\text{O}_{64}-\text{O}_{150}]$ ; (c) distance between  $\text{Ser}_{64}\text{O}_\gamma$  and  $\text{Lys}_{67}\text{N}_\eta$ ,  $d[\text{O}_{64}-\text{N}_{67}]$ . In the structure  $\text{Tyr150A}^-$ , the coordinate  $C[\text{H}_{64}-\text{O}_{150}] \approx 0$ . Since a proton transfer from

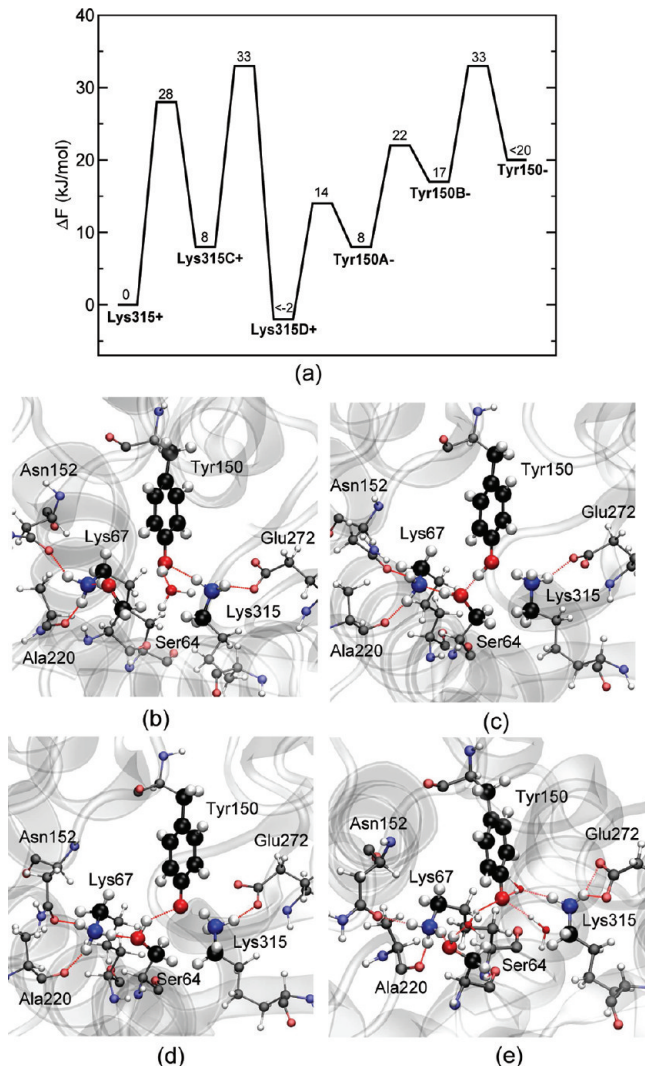


**Figure 10.** (a) Free energy profile for the transition from **Lys315+** → **Tyr150-**. Active site structures of intermediates observed during this process are also shown: (b) **Lys315C+**, (c) **Lys315D+**, (d) **Tyr150A-**, and (e) **Tyr150B-**.

$\text{Ser}_{64}\text{O}_\gamma$  to  $\text{Tyr}_{150}\text{O}_\eta$  can take the system back to **Lys315D+**, we set a wall at position  $\text{C}[\text{H}_{64}-\text{O}_{150}] \approx 0.45$  to prevent  $\text{Tyr150A-} \rightarrow \text{Lys315D+}$ . The other two collective coordinates,  $d[\text{O}_{64}-\text{O}_{150}]$  and  $d[\text{O}_{64}-\text{N}_{67}]$  were chosen for accelerating the breakage of hydrogen bonds  $\text{Tyr}_{150}\text{O}_\eta \cdots \text{Ser}_{64}\text{H}_\gamma$  and  $\text{Lys}_{67}\text{N}_\eta \cdots \text{Ser}_{64}\text{O}_\gamma$  in order to eventually form **Tyr150-**. From the metadynamics trajectory, it was observed that the hydrogen bond between  $\text{Ser}_{64}\text{H}_\gamma$  and  $\text{Tyr}_{150}\text{O}_\eta$  breaks, followed by the reorientation of  $\text{Ser}_{64}\text{H}_\gamma$  toward a water molecule. In this structure, **Tyr150B-**,  $\text{Tyr}_{150}\text{O}_\eta$  retained its hydrogen bond with a water molecule, as in **Tyr150A-**, but has an additional weak hydrogen bonding with a water molecule (see Figure 10e). The residue  $\text{Lys}_{315}$  is still far from  $\text{Tyr}_{150}$  and remains hydrogen-bonded with  $\text{Glu}_{272}$ . The free energy barrier for  $\text{Tyr150A-} \rightarrow \text{Tyr150B-}$  is only about 14 kJ/mol, and the reverse barrier is nearly 5 kJ/mol; see Figure 10a, and also FigSI 4.

Yet, the structure **Tyr150B-** is quite different from **Tyr150-**, in particular, in the alignment of  $\text{Lys}_{67}$  and  $\text{Lys}_{315}$ . To form **Tyr150-** from **Tyr150B-**,  $\text{Lys}_{67}$  should break the hydrogen-bonding interaction with  $\text{Ser}_{64}$  and then twist around the  $\text{C}_\delta-\text{C}_\epsilon$  bond of  $\text{Lys}_{67}$  such that the  $\text{Lys}_{67}\text{H}_\zeta$  get closer to  $\text{Tyr}_{150}\text{O}_\eta$ .

Moreover,  $\text{Lys}_{315}$  needs to reorient toward  $\text{Tyr}_{150}$ . We found that at least four collective coordinates are required to sample this process using metadynamics: Distances between (a)  $\text{Ser}_{64}\text{O}_\gamma$  and  $\text{Lys}_{67}\text{N}_\zeta$ ,  $d[\text{O}_{64}-\text{N}_{67}]$ , (b)  $\text{Lys}_{67}\text{N}_\zeta$  and  $\text{Tyr}_{150}\text{O}_\eta$ ,  $d[\text{O}_{150}-\text{N}_{67}]$ , (c)  $\text{Lys}_{67}\text{N}_\zeta$  and  $\text{Tyr}_{150}\text{O}_\eta$ ,  $d[\text{O}_{150}-\text{O}_{64}]$ , and (d)  $\text{Ser}_{64}\text{O}_\gamma$  and  $\text{Tyr}_{150}\text{O}_\eta$ ,  $d[\text{O}_{150}-\text{O}_{64}]$ . Unfortunately, using these four distance collective coordinates in a QM/MM simulation requires unaffordably long computing time to sample the underlying free energy landscape. Since the structural change from  $\text{Tyr150B-} \rightarrow \text{Tyr150-}$  involves only breakage of hydrogen bonds and structural rearrangements, we can conveniently simulate the process using classical force field, instead of using the computationally expensive QM/MM method. On carrying out this metadynamics simulation, we found that at first the hydrogen bond between  $\text{Ser}_{64}\text{O}_\gamma$  and  $\text{Lys}_{67}\text{N}_\zeta$  breaks, followed by twisting about the  $\text{C}_\delta-\text{C}_\epsilon$  bond of  $\text{Lys}_{67}$ . Immediately,  $\text{Lys}_{315}$  moves toward the  $\text{Tyr}_{150}$  resulting in **Tyr150-** structure. The free energy barrier to surmount for  $\text{Tyr150B-} \rightarrow \text{Tyr150-}$  is only 16 kJ/mol; free energy surface for this process is available in FigSI 5. Thus, the effective barrier in going from **Lys315+** → **Tyr150-** is only about 33 kJ/mol.

### 3.5. Effect of Noncovalently Complexed Cephalothin Drug Molecule on the Protonation States.

To scrutinize the effect of cephalothin molecule on the kinetic and thermodynamic stability of the active site protonation states of  $\text{C}\beta$ -lactamase active site, we also looked into the proton transfer dynamics in drug–enzyme noncovalent complex.

In the empirical force-field simulation of the drug–enzyme complex with **Tyr150-** protonation state, carried out prior to the metadynamics simulation, the complex remained stable only for 2.4 ns (1 ns *NPT* + 1.4 ns *NVT*), after which the cephalothin molecule partially lost its interaction with  $\text{Ser}_{64}$  and tilted away from the active site (see also FigSI 6). Interestingly, before the detachment, the structure of the drug–enzyme complex in **Tyr150-** protonation state, labeled as **Tyr150Cep-**, resembled the X-ray structure (1KVL<sup>53</sup>); see the Supporting Information for more details and Figure 11a. In this structure,

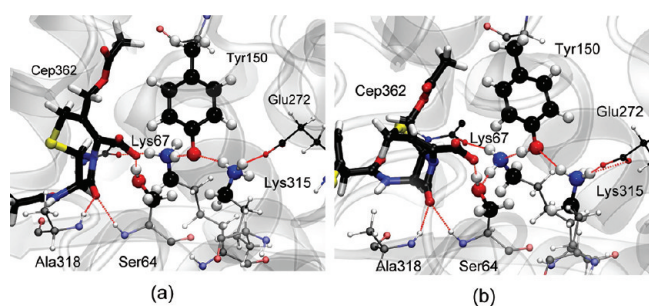


**Figure 11.** Average active site structure (a) **Tyr150Cep-** and (b) **Lys315Cep+** obtained from empirical force field based MD simulation. Cephalothin molecule is rendered here in thick cylinders.

$\text{Ser}_{64}$  is well positioned to attack the carbonyl group of  $\beta$ -lactam ring; the average distance between  $\text{Cep}_{362}\text{C}_9$  and  $\text{Ser}_{64}\text{O}_\gamma$  is 3.02 Å. Notably,  $\text{Ser}_{64}\text{H}_\gamma$  is hydrogen bonded to the carboxylate group of  $\text{Cep}_{362}$ ;  $d[\text{Ser}_{64}\text{H}_\gamma \cdots \text{Cep}_{362}\text{O}_4] = 1.81$  Å. On the other hand, the drug–enzyme complex having the **Lys315+** protonation state, hereafter called **Lys315Cep+**, was stable during the entire 5 ns *NVT* simulation (Figure 11b). Like in the case of **Tyr150Cep-**,  $\text{Ser}_{64}\text{H}_\gamma$  features a hydrogen bond interaction with  $\text{Cep}_{362}\text{O}_4$ , and  $\text{Ser}_{64}$  is well positioned to attack the beta-lactam ring;  $d[\text{Cep}_{362}\text{C}_9 \cdots \text{Ser}_{64}\text{O}_\gamma] = 2.96$  Å. A

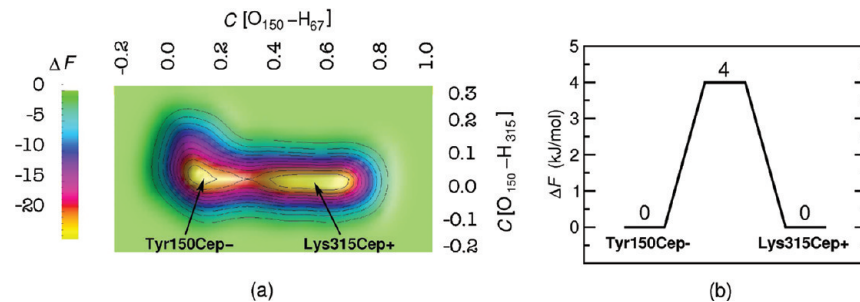


**Figure 12.** Free energy surface (a) and free energy profile (b) for the process  $\text{Tyr150Cep}^- \rightleftharpoons \text{Lys315Cep}^+$ .

noticeable difference with the apoenzyme  $\text{Lys315}^+$  protonation state is that  $\text{Tyr}_{150}\text{H}_\eta$  is hydrogen bonded to  $\text{Lys}_{67}\text{N}_\zeta$ . A stable contact between oxyanions hole and carbonyl group of cephalothin is observed in both  $\text{Tyr150Cep}^-$  and  $\text{Lys315Cep}^+$ . They are in favor of a “substrate facilitated” acylation mechanism, where carboxylate group of the cephalothin drug abstract  $\text{Ser}_{64}\text{H}_\gamma$ , thereby activating the  $\text{Ser}_{64}$  for nucleophilic attack.

In order to gauge the stability of  $\text{Tyr150Cep}^-$  and  $\text{Lys315Cep}^+$ , the free energy barrier for proton transfer between the  $\text{Tyr}_{150}\text{O}_\eta$  and  $\text{Lys}_{315}\text{H}_\zeta$  was obtained using metadynamics QM/MM simulations. Interestingly, even in an NVT ensemble QM/MM simulation of  $\text{Lys315Cep}^+$ , which was done prior to metadynamics simulation, proton transfer between  $\text{Tyr}_{150}\text{O}_\eta$  and  $\text{Lys}_{67}\text{N}_\zeta$  has been observed several times, i.e., the process  $\text{Tyr150Cep}^- \rightleftharpoons \text{Lys315Cep}^+$  (see FigSI 7b). This indicates that both the forward and reverse free energy barriers for the process  $\text{Tyr150Cep}^- \rightleftharpoons \text{Lys315Cep}^+$  are only of the order a few  $k_\text{B}T_{300\text{K}}$ . However, no proton transfer between  $\text{Lys}_{315}$  and  $\text{Tyr}_{150}$  was seen, unlike in the case of the apoenzyme. All other interactions in the active site remained intact throughout this simulation.

As a next step, we employed the metadynamics technique to quantify the free energy barriers involving the proton transfer dynamics  $\text{Tyr150Cep-Lys315Cep}^+$ . We chose two collective coordinates: (a) coordination number of  $\text{Tyr}_{150}\text{O}_\eta$  to all three  $\text{Lys}_{67}\text{H}_\zeta$ ,  $C[\text{O}_{150}-\text{H}_{67}]$  and (b) coordination number of  $\text{Tyr}_{150}\text{O}_\eta$  to the three hydrogens  $\text{Lys}_{315}\text{H}_\zeta$ , where sampling of  $C[\text{O}_{150}-\text{H}_{315}]$  was restricted below 0.4 using a wall potential. The forward and the reverse processes, i.e.,  $\text{Tyr150Cep}^- \rightarrow \text{Lys315Cep}^+$  and  $\text{Lys315Cep}^+ \rightarrow \text{Tyr150Cep}^-$ , respectively, occurred multiple times during the metadynamics simulation. The reconstructed free energy surface from this simulation is shown in Figure 12. Interestingly, the free energy barrier for both the forward and the reverse process is the same and is only 4 kJ/mol, which is in agreement with the frequent proton transfer observed in the NVT simulation. Moreover, free energy surface also indicates that  $\text{Tyr150Cep}^-$  and  $\text{Lys315Cep}^+$  are having the same free energy.

The substantial change in the free energy barrier due to complexing with the drug molecule can be ascribed to the structural changes occurring at the active site. Especially, the hydrogen bond formed between  $\text{Ser}_{64}\text{H}_\gamma$  and the carboxylate group of the drug molecule results in weakening the  $\text{Ser}_{64}$  interaction with  $\text{Lys}_{67}$ , which in turn facilitates a stronger  $\text{Lys}_{67}\text{H}_\zeta \cdots \text{Tyr}_{150}\text{O}_\eta$  interaction; see also FigSI 7a.

#### 4. DISCUSSION

Series of MM and QM/MM molecular dynamics simulations were performed to scrutinize the kinetic and thermodynamic

stability of three protonation states of the active site. The  $\text{Lys67}^+$  protonation state is excluded based on the fact that the equilibrium structure of  $\text{Lys67}^+$  is largely deviating from the X-ray structure of the apoprotein, and basic  $\text{Lys}_{315}$  structure is not in an appropriate conformation to delocalize a proton from  $\text{Ser}_{64}$ . This result agrees with previous free energy calculations.<sup>38,46,49</sup>

The average  $\text{Tyr150}^-$  structure, on the other hand, matches well with the reported X-ray structure of the apoenzyme (Table 2). Notably, the crucial  $\text{Ser}_{64}$  residue has no direct interaction with  $\text{Tyr}_{150}\text{O}_\eta$ . Our QM/MM molecular simulations of  $\text{Tyr150}^-$  protonation state of the solvated protein at ambient conditions showed that, at equilibrium, the proton  $\text{Lys}_{315}\text{H}_\zeta$  is largely delocalized between the  $\text{Tyr}_{150}\text{O}_\eta$  and  $\text{Lys}_{315}\text{N}_\zeta$ . Although, hydrogen–bonding interaction exists between  $\text{Tyr}_{150}\text{O}_\eta$  and  $\text{Lys}_{67}\text{H}_\zeta$ , no proton transfer was observed during the canonical ensemble simulation. Metadynamics simulations, however, indicated that the  $\text{Tyr150}^- \rightarrow \text{Lys315}^+$  proton transfer process involves overcoming a free energy barrier of about 94 kJ/mol. This process proceeds through the  $\text{Lys315}^+$  minimum energy structure, in which a proton transfer from  $\text{Lys}_{67}\text{N}_\zeta$  to  $\text{Tyr}_{150}\text{O}_\eta$  has already taken place. A high free energy barrier is a result of the structural changes in the subsequent steps involved in attaining the equilibrium  $\text{Lys315}^+$  structure.

Formation of  $\text{Lys315}^+$  structure from  $\text{Tyr150}^-$  results in rearrangements of the active site residues and hydrogen bonding patterns. Therefore, the reverse process, i.e.,  $\text{Lys315}^+ \rightarrow \text{Tyr150}^-$ , goes through a different pathway than the forward process. We observed an indirect proton transfer from  $\text{Tyr}_{150}\text{O}_\eta$  to  $\text{Lys}_{67}\text{N}_\zeta$  through  $\text{Ser}_{64}$ . Very interestingly, in the  $\text{Lys315}^+$  state,  $\text{Tyr}_{150}$  is quite flexible and it forms a direct hydrogen bond with  $\text{Ser}_{64}$ . Simultaneous proton transfer from  $\text{Ser}_{64}\text{H}_\gamma$  to  $\text{Lys}_{67}\text{N}_\zeta$  followed by  $\text{Tyr}_{150}\text{H}_\eta$  to  $\text{Ser}_{64}\text{O}_\gamma$  was observed during the simulation. The net free energy for this multistep process is about 33 kJ/mol.

The overall process can be visualized as a cycle, as shown in Figure 13. Along this cyclic route, the  $\text{Tyr150}^-$  structure is thermodynamically more stable than  $\text{Lys315}^+$  structure. Although the exact free energy difference cannot be estimated based on the current work, one can conclude that  $\text{Lys315}^+$  is at least 61 kJ/mol higher in energy than  $\text{Tyr150}^-$ . The process  $\text{Tyr150}^- \rightarrow \text{Lys315}^+$  can happen at millisecond time scales, whereas the latter cycles back to  $\text{Tyr150}^-$  in a few microseconds at ambient conditions. This implies that the  $\text{Lys315}^+$  configuration is kinetically unstable and there is a higher probability in finding  $\text{Tyr150}^-$  compared to  $\text{Lys315}^+$ . The thermodynamic stability of  $\text{Tyr150}^-$  agrees with numerous experimental works.<sup>14,36,39–41</sup>

Previous theoretical calculations by Díaz et al.<sup>49</sup> have also predicted a lower energy for the  $\text{Tyr150}^-$  in comparison to

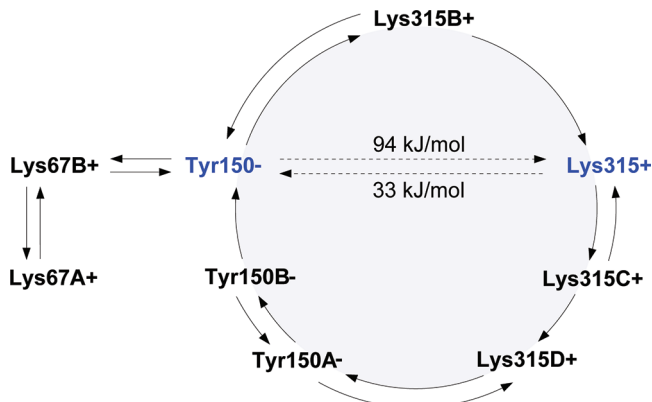


**Figure 13.** Proton transfer pathway for  $\text{Tyr150}^- \rightleftharpoons \text{Lys315}^+$  process. The entire process can be seen as a cyclic process. Effective free energy barriers are shown above the dotted arrows.

**Lys315<sup>+</sup>**, but only by 4 kJ/mol. It is also noted in passing that the equilibrium **Lys315<sup>+</sup>** structure that we obtained in classical force field and QM/MM metadynamics simulations is different to that which was reported by Díaz et al.<sup>49</sup> The difference in the free energy estimate may originate from the disparities in the techniques followed, in particular, the static PM3 semiempirical approach used in ref 49. Moreover, **Tyr150<sup>-</sup>** has its proton delocalized between  $\text{Tyr}_{150}$  and  $\text{Lys}_{315}$ , and thus its free energy comprises of significant entropy.

Proton transfer to  $\text{Lys}_{67}$ , i.e., the formation of structure **Lys315B<sup>+</sup>** from **Tyr150<sup>-</sup>**, needs to overcome a free energy barrier of about 31 kJ/mol, which could take place in a few tens of nanosecond at 300 K. The net population of **Lys315B<sup>+</sup>** will be still lower due to a low reverse barrier. By the presence of **Lys67A<sup>+</sup>**, **Lys67B<sup>+</sup>**, and **Lys315B<sup>+</sup>** states that are accessible in short time scales from the **Tyr150<sup>-</sup>** protonation state, the  $\text{Tyr}_{150}$  will not be always in a fully deprotonated state at ambient conditions. This agrees with the experimental observations of Ishiguro et al.,<sup>42</sup> although the authors concluded co-existence of a protonated  $\text{Lys}_{67}$ , protonated  $\text{Tyr}_{150}$ , and protonated  $\text{Lys}_{315}$ . We believe that in their experiments the change in the chemical shift observed around pH 8.3 is due to the proton transfer from  $\text{Tyr}_{150}\text{O}_\eta$  to  $\text{OH}^-$  when the protonation state of the active site is either **Lys67A<sup>+</sup>**, **Lys67B<sup>+</sup>**, or **Lys315B<sup>+</sup>**. The resulting structure may then rearrange, followed by a proton transfer to  $\text{Tyr}_{150}\text{O}_\eta$  from either  $\text{Lys}_{67}$  or  $\text{Lys}_{315}$ . The further abstraction of this proton from  $\text{Tyr}_{150}\text{O}_\eta$  may then correspond to the change in chemical shift observed at pH 11 in ref 42.

Our observations are also in line with the fact that the  $\text{pK}_a$  values of  $\text{Tyr}_{150}$  are lower than those in solution due to the proximity of positively charged  $\text{Lys}_{67}$  and  $\text{Lys}_{315}$ .<sup>39</sup> Although we cannot fully rule out the possibility of all three residues being protonated as proposed by Ishiguro et al.<sup>42</sup> and calculations of Bandyopadhyay,<sup>94</sup> the comparison of equilibrium structure of such a protonation state is reported to show large deviations from the X-ray structure of the apoenzyme.<sup>49,94</sup>

However, a cooperative effect of the  $\text{Tyr}_{150}$ ,  $\text{Lys}_{67}$ , and  $\text{Lys}_{315}$  is obvious from our studies. This work also supports a facile proton relay mechanism at the active site.<sup>17</sup>

Finally, our study shows that the kinetic and thermodynamic stabilities of protonation states vary by the structural changes at the active site as a result of noncovalent ligation of the cephalothin drug molecule. Binding of the molecule results in noticeable structural changes, resulting in lowering free energy

barriers and free energy differences by 1 order of magnitude and up to  $10^{14}$  fold increase in proton transfer rate. In the drug–enzyme complex, **Tyr150<sup>-</sup>** and **Lys315<sup>+</sup>** become equally stable, and the kinetic barrier separating them is only of the order of  $2 k_B T_{300K}$ . This implies that both protonation states are equally likely and kinetically accessible in the presence of the drug molecule. Change in free energies of protonation states in the presence of drug molecule has been observed in all previous theoretical works on the topic.<sup>38,46,49,94</sup> Our result is also in line with notable stabilization of **Lys315<sup>+</sup>** in a pre-covalent drug–enzyme complex.<sup>49</sup> Some of the previous theoretical studies have reported that **Tyr150<sup>-</sup>** is the stable protonation state in the (covalently complexed) acyl–enzyme intermediate structures. High resolution X-ray structures of boronic acid deacylation intermediates implied the presence of a protonated form of  $\text{Tyr}_{150}$ .<sup>43</sup> Our calculations show that, in the presence of noncovalently bound cephalothin, positions of heavy atoms are nearly the same for **Tyr150<sup>-</sup>** and **Lys315<sup>+</sup>** protonation states, and therefore, interpretation of protonation states solely based on the X-ray structure can be misleading.

Of great importance toward understanding the acylation mechanism, it is observed that both **Tyr150<sup>-</sup>** and **Lys315<sup>+</sup>** protonation states have  $\text{Cep}_{362}\text{C}_9$  and  $\text{Ser}_{64}\text{O}_\gamma$  positioned at a convenient distance ( $\sim 3 \text{ \AA}$ ) for the acylation reaction. Further, the hydrogen bond between  $\text{Ser}_{64}\text{H}_\gamma$  and carboxylate group of cephalothin ( $\text{Cep}_{362}\text{O}_{4A}$ ) supports a “substrate assisted” acylation mechanism where  $\text{Ser}_{64}\text{O}_\gamma$  is activated by the transfer of  $\text{Ser}_{64}\text{H}_\gamma$  to  $\text{Cep}_{362}\text{O}_{4A}$ .

## 5. CONCLUSIONS

A detailed study of thermodynamic and kinetic stability of various protonation states of the active site residues of an class C  $\beta$ -lactamase is presented here employing hybrid QM/MM molecular dynamics techniques. In the absence of antibiotic molecule, the three different protonation states for the active site residues  $\text{Tyr}_{150}$ ,  $\text{Lys}_{67}$ , and  $\text{Lys}_{315}$  have significantly distinct equilibrium structures. Among them, the kinetically and thermodynamically most stable one is **Tyr150<sup>-</sup>** structure where  $\text{Tyr}_{150}$  is deprotonated,  $\text{Lys}_{67}$  is protonated, and  $\text{Lys}_{315}$  is protonated, and resembles well the X-ray structural data. At room temperature, **Tyr150<sup>-</sup>** has a dynamic structure, where one of the protons of  $\text{Lys}_{315}\text{N}_\zeta$  is delocalized between  $\text{Lys}_{315}\text{N}_\zeta$  and  $\text{Tyr}_{150}\text{O}_\eta$ . Formation of the **Lys315<sup>+</sup>** structure, where  $\text{Tyr}_{150}$  and  $\text{Lys}_{315}$  are protonated but  $\text{Lys}_{67}$  is neutral, has to overcome a free energy barrier of about 94 kJ/mol, whereas the reverse barrier is only one-third in magnitude. Interestingly, forward and reverse processes of  $\text{Tyr150}^- \rightleftharpoons \text{Lys315}^+$  proceed through different reaction pathways. Overall the proton transfer process  $\text{Tyr150}^- \rightleftharpoons \text{Lys315}^+$  can be considered as cyclic, which traversed many intermediates that have distinctly different structures. A cooperative effect of  $\text{Tyr}_{150}$ ,  $\text{Lys}_{67}$ , and  $\text{Lys}_{315}$  residues was observed during the proton transfer dynamics, and thus a facile proton relay mechanism at the active site is conceivable, which may be important for the reaction with antibiotics. The stabilities of protonation states of the enzyme are largely altered upon noncovalently complexing with a cephalothin antibiotic molecule. The structural changes associated by the interaction with the drug molecule result in the decrease of the forward and the backward free energy barrier for  $\text{Tyr150}^- \rightleftharpoons \text{Lys315}^+$  to only 4 kJ/mol. This implies that both protonation states are thermally accessible in the presence of the drug molecule. In drug–enzyme complex of both protonation states, the  $\text{Ser}_{64}\text{O}_\gamma$  and the  $\beta$ -lactam ring of

the antibiotic are positioned favorably for a nucleophilic attack of Ser<sub>64</sub>O<sub>γ</sub> on the β-lactam ring. The hydrogen bond between Ser<sub>64</sub>H<sub>γ</sub> and the carboxylate group of cephalothin (Cep<sub>362</sub>O<sub>4A</sub>) suggest the possibility of a substrate assisted activation of Ser<sub>64</sub>.

## ■ ASSOCIATED CONTENT

### S Supporting Information

rmsd analysis, reconstructed free energy surfaces, three-dimensional structures and bond–distance analysis. PDB files of the protein structure after the classical canonical ensemble simulations for the Tyr150– and Lys315+ protonation states, for both the apoenzyme and with the cephalothin drug molecule, are deposited. Charges computed using for Tyr<sub>150</sub>– residue and the cephalothin drug molecule are also present. Cartesian coordinates of the minimum and transition state structures used for benchmarking the PBE functionals are available. This material is available free of charge via the Internet at <http://pubs.acs.org>.

## ■ AUTHOR INFORMATION

### Corresponding Author

\*E-mail: nnair@iitk.ac.in.

### Notes

The authors declare no competing financial interest.

## ■ ACKNOWLEDGMENTS

Calculations were performed using the ChemFIST computer cluster (Department of Chemistry) and the HPC facility at IIT Kanpur. R.T. acknowledges the Council of Scientific and Industrial Research (CSIR), India, and IIT Kanpur for his Ph.D. fellowship.

## ■ REFERENCES

- (1) Sanders, C. C.; Sanders, W. E. *Eur. J. Clin. Microbiol.* **1987**, *6*, 435–437.
- (2) Fong, I. W.; Drlica, K., Eds. *Antimicrobial resistance and implications for the 21st century*. Springer Science+Business Media, LLC: New York, 2008.
- (3) Paterson, D. L.; Bonomo, R. A. *Clin. Microbiol. Rev.* **2005**, *18*, 657–686.
- (4) Bradford, P. *Clin. Microbiol. Rev.* **2001**, *14*, 933–951.
- (5) Jacoby, G. A.; Medeiros, A. A. *Antimicrob. Agents Chemother.* **1991**, *35*, 1697–1704.
- (6) Walsh, T. R.; Toleman, M. A.; Poirel, L.; Nordmann, P. *Clin. Microbiol. Rev.* **2005**, *18*, 306–325.
- (7) Fisher, J. F.; Meroueh, S. O.; Mobashery, S. *Chem. Rev.* **2005**, *105*, 395–424.
- (8) Cavalli, A.; Carloni, P.; Recanatini, M. *Chem. Rev.* **2005**, *106*, 3497–3519.
- (9) Bulychev, A.; Massova, I.; Miyashita, K.; Mobashery, S. *J. Am. Chem. Soc.* **1997**, *119*, 7619–7625.
- (10) Fenollar-Ferrer, C.; Donoso, J.; Frau, J.; Muñoz, F. *Chem. Biodiversity* **2005**, *2*, 645–656.
- (11) Chen, Y.; McReynolds, A.; Shoichet, B. K. *Protein Sci.* **2009**, *18*, 662–669.
- (12) Monnaie, D.; Dubus, A.; Frère, J.-M. *Biochem. J.* **1994**, *302*, 1–4.
- (13) Dubus, A.; Ledent, P.; Lamotte-Brasseur, J.; Frère, J.-M. *Proteins: Struct., Funct., Genet.* **1996**, *25*, 473–485.
- (14) Page, M. I.; Vilanova, B.; Layland, N. *J. Am. Chem. Soc.* **1995**, *117*, 12092–12095.
- (15) Usher, K. C.; Blaszcak, L. C.; Weston, G. S.; Shoichet, B. K.; Remington, S. J. *Biochemistry* **1998**, *37*, 16082–16092.
- (16) Dubus, A.; Normark, S.; Kania, M.; Page, M. G. P. *Biochemistry* **1994**, *33*, 8577–8586.
- (17) Goldberg, S. D.; Iannuccilli, W.; Nguyen, T.; Ju, J.; Cornish, V. *W. Protein Sci.* **2003**, *12*, 1633–1645.
- (18) Majiduddin, F. K.; Materon, I. C.; Palzkill, T. G. *Int. J. Med. Microbiol.* **2002**, *292*, 127–137.
- (19) Livermore, D. M. *Clin. Microbiol. Rev.* **1995**, *8*, 557–584.
- (20) Sanders, C. C.; Sanders, W. E. *Clin. Infectious Disease* **1992**, *15*, 824–839.
- (21) Knowles, J. R. *Acc. Chem. Res.* **1985**, *18*, 97–104.
- (22) Frère, J.-M. *Mol. Microbiol.* **1995**, *16*, 385–395.
- (23) Tenover, F. C. *Clin. Infectious Disease* **2001**, *33*, S108–S115.
- (24) Ambler, R. P. *Phil. Trans. R. Soc. London B* **1980**, *289*, 321–331.
- (25) Livermore, D. M.; Woodford, N. *Curr. Opin. Microbiol.* **2000**, *3*, 489–495.
- (26) Fenollar-Ferrer, C.; Frau, J.; Donoso, J.; Muñoz, F. *Theor. Chem. Acc.* **2008**, *121*, 209–218.
- (27) Beceiro, A.; Bou, G. *Rev. Med. Micro.* **2004**, *15*, 141–152.
- (28) Knott-Hunziker, V.; Petrusson, S.; Waley, S. G.; Jaurin, B.; Grundstrom, T. *Biochem. J.* **1982**, *207*, 315–322.
- (29) Pratt, R. F. *Science* **1989**, *246*, 917–919.
- (30) Nukaga, M.; Haruta, S.; Tanimoto, K.; Kogure, K.; Taniguchi, K.; Tamaki, M.; Sawai, T. *J. Biol. Chem.* **1995**, *270*, 5729–5735.
- (31) Powers, R. A.; Shoichet, B. K. *J. Med. Chem.* **2002**, *45*, 3222–3234.
- (32) Rahil, J.; Pratt, R. F. *Biochemistry* **1992**, *31*, 5869–5878.
- (33) Tsukamoto, K.; Tachibana, K.; Yamazaki, N.; Ishii, Y.; Ujiie, K.; Nishida, N.; Sawai, T. *Eur. J. Biochem.* **1990**, *188*, 15–22.
- (34) Tsukamoto, K.; Nishida, N.; Tsuruoka, M.; Sawai, T. *FEBS Lett.* **1990**, *271*, 243–246.
- (35) Monnaie, D.; Dubus, A.; Cooke, D.; Marchand-Brynaert, J.; Normark, S.; Frère, J.-M. *Biochemistry* **1994**, *33*, 5193–201.
- (36) Oefner, C.; D'Arcy, A.; Daly, J. J.; Gubernator, K.; Charnas, R. L.; Heinze, I.; Hubschwerlen, C.; Winkler, F. K. *Nature* **1990**, *343*, 284–288.
- (37) Beadle, B. M.; Trehan, I.; Focia, P. J.; Shoichet, B. K. *Structure* **2002**, *10*, 413–424.
- (38) Hata, M.; Tanaka, Y.; Fujii, Y.; Neya, S.; Hoshino, T. *J. Phys. Chem. B* **2005**, *109*, 16153–16160.
- (39) Lamotte-Brasseur, J.; Dubus, A.; Wade, R. C. *Proteins: Struct., Funct., Genet.* **2000**, *40*, 23–28.
- (40) Lobkovsky, E.; Moews, P. C.; Liu, H.; Zhao, H.; Frère, J.-M.; Knox, J. R. *Proc. Natl. Acad. Sci.* **1993**, *90*, 11257–11261.
- (41) Patera, A.; Blaszcak, L. C.; Shoichet, B. K. *J. Am. Chem. Soc.* **2000**, *122*, 10504–10512.
- (42) Kato-Toma, Y.; Iwashita, T.; Masuda, K.; Oyama, Y.; Ishiguro, M. *Biochem. J.* **2003**, *371*, 175–181.
- (43) Chen, Y.; Minasov, G.; Roth, T. A.; Prati, F.; Shoichet, B. K. *J. Am. Chem. Soc.* **2006**, *128*, 2970–2976.
- (44) Fenollar-Ferrer, C.; Frau, J.; Donoso, J.; Muñoz, F. *Proteins: Struct., Funct., Genet.* **2003**, *51*, 442–452.
- (45) Dall'acqua, W.; Carter, P. *Protein Sci.* **2000**, *9*, 1–9.
- (46) Gherman, B. F.; Goldberg, S. D.; Cornish, V. W.; Friesner, R. A. *J. Am. Chem. Soc.* **2004**, *126*, 7652–7664.
- (47) Schutz, C. N.; Warshel, A. *Proteins: Struct., Funct., Genet.* **2001**, *44*, 400–417.
- (48) Isom, D. G.; Castañeda, C. A.; Cannon, B. R.; Gracia-Moreno, E. B. *Proc. Natl. Acad. Sci.* **2011**, *108*, 5260–5265.
- (49) Díaz, N.; Suárez, D.; Sordo, T. L. *Biochemistry* **2006**, *45*, 439–451.
- (50) Marx, D.; Hutter, J. *Ab Initio Molecular Dynamics: Basic Theory and Advanced Methods*. Cambridge University Press: Cambridge, U.K., 2009.
- (51) Case, D. A.; Darden, T. A.; Cheatham III, T. E.; Simmerling, C. L.; Wang, J.; Duke, R. E.; Luo, R.; Walker, R. C.; Zhang, W.; K.M. Merz, B. R.; Wang, B.; Hayik, S.; Roitberg, A.; Seabra, G.; Kolossvai, I.; Wong, K. F.; Paesani, F.; Vanicek, J.; Liu, J.; Wu, X.; Brozell, S. R.; Steinbrecher, T.; Gohlke, H.; Cai, Q.; Ye, X.; Wang, J.; Hsieh, M.-J.; Cui, G.; Roe, D.; Mathews, D. H.; Seetin, M. G.; Sagui, C.; Babin, V.; Luchko, T.; Gusalov, S.; Kovalenko, A.; Kollman, P. *AMBER 11*. University of California: San Francisco, 2010.

- (52) Michaux, C.; Charlier, P.; Frère, J.-M.; Wouters, J. *J. Am. Chem. Soc.* **2005**, *127*, 3262–3263.
- (53) Beadle, B. M.; Trehan, I.; Focia, P. J.; Shoichet, B. K. *Structure* **2002**, *10*, 413–424.
- (54) Laio, A.; Parrinello, M. *Proc. Natl. Acad. Sci.* **2002**, *99*, 12562–12566.
- (55) Iannuzzi, M.; Laio, A.; Parrinello, M. *Phys. Rev. Lett.* **2003**, *90*, 238302–1–4.
- (56) Version 9.9. *Modeller: Program for Comparative Protein Structure Modelling by Satisfaction of Spatial Restraints*. see also <http://salilab.org/modeller>.
- (57) Cheatham, T. E.; Cieplak, P.; Kollman, P. A. *J. Biomol. Struct. Dyn.* **1999**, *16*, 845–62.
- (58) Version III.3. *RED: RESP ESP charge Derive*. See also <http://q4md-forcefieldtools.org/RED/>.
- (59) Wang, J.; Wolf, R. M.; Caldwell, J. W.; Kollman, P. A.; Case, D. A. *J. Comput. Chem.* **2004**, *25*, 1157–1173.
- (60) Version 13.2. *CPMD Program Package*. IBM Corp 1990–2011, MPI für Festkörperforschung Stuttgart 1997–2001. See also <http://www.cpmd.org>.
- (61) Martyna, G. J.; Tuckerman, M. E. *J. Chem. Phys.* **1999**, *110*, 2810–2821.
- (62) Laio, A.; VandeVondele, J.; Rothlisberger, U. *J. Chem. Phys.* **2002**, *116*, 6941–6947.
- (63) Perdew, J. P.; Chevary, J. A.; Vosko, S. H.; Jackson, K. A.; Pederson, M. R.; Singh, D. J.; Fiolhais, C. *Phys. Rev. B* **1992**, *46*, 6671–6687.
- (64) Vanderbilt, D. *Phys. Rev. B* **1990**, *41*, 7892–7895.
- (65) Car, R.; Parrinello, M. *Phys. Rev. Lett.* **1985**, *55*, 2471–2474.
- (66) Martyna, G. J.; Klein, M. L.; Tuckerman, M. *J. Chem. Phys.* **1992**, *97*, 2635–2643.
- (67) Ensing, B.; Vivo, M. D.; Liu, Z.; Moore, P.; Klein, M. L. *Acc. Chem. Res.* **2006**, *39*, 73–81.
- (68) Barducci, A.; Bonomi, M.; Parrinello, M. *WIREs Comput. Mol. Sci.* **2011**, *1*, 826–843.
- (69) Nair, N. N. *J. Phys. Chem. B* **2011**, *115*, 2312–2321.
- (70) Ensing, B.; Laio, A.; Parrinello, M.; Klein, M. L. *J. Phys. Chem. B* **2005**, *109*, 6676–6687.
- (71) Nair, N. N.; Schreiner, E.; Marx, D. *J. Am. Chem. Soc.* **2006**, *128*, 13815–13826.
- (72) Ireta, J.; Neugebauer, J.; Scheffler, M. *J. Phys. Chem. A* **2004**, *108*, 5692–5698.
- (73) Nygaard, T. P.; Alfonso-Prieto, M.; Peters, G. H.; Jensen, M.; Rovira, C. *J. Phys. Chem. B* **2010**, *114*, 11859–11865.
- (74) Jensen, M.; Rothlisberger, U.; Rovira, C. *Biophys. J.* **2005**, *89*, 1744–1759.
- (75) Petersen, L.; Ardevol, A.; Rovira, C.; Reilly, P. J. *J. Phys. Chem. B* **2009**, *113*, 7331–7339.
- (76) Lynch, B. J.; Fast, P. L.; Harris, M.; Truhlar, D. G. *J. Phys. Chem. A* **2000**, *104*, 4811–4815.
- (77) Lynch, B. J.; Zhao, Y.; Truhlar, D. G. *J. Phys. Chem. A* **2003**, *107*, 1384–1388.
- (78) Frisch, M. J.; Trucks, G. W.; Schlegel, H. B.; Scuseria, G. E.; Robb, M. A.; Cheeseman, J. R.; Scalmani, G.; Barone, V.; Mennucci, B.; Petersson, G. A.; Nakatsuji, H.; Caricato, M.; Li, X.; Hratchian, H. P.; Izmaylov, A. F.; Bloino, J.; Zheng, G.; Sonnenberg, J. L.; Hada, M.; Ehara, M.; Toyota, K.; Fukuda, R.; Hasegawa, J.; Ishida, M.; Nakajima, T.; Honda, Y.; Kitao, O.; Nakai, H.; Vreven, T.; J. A. Montgomery, J.; Peralta, J. E.; Ogliaro, F.; Bearpark, M.; Heyd, J. J.; Brothers, E.; Kudin, K. N.; Staroverov, V. N.; Keith, T.; Kobayashi, R.; Normand, J.; Raghavachari, K.; Rendell, A.; Burant, J. C.; Iyengar, S. S.; Tomasi, J.; Cossi, M.; Rega, N.; Millam, J. M.; Klene, M.; Knox, J. E.; Cross, J. B.; Bakken, V.; Adamo, C.; Jaramillo, J.; Gomperts, R.; Stratmann, R. E.; Yazyev, O.; Austin, A. J.; Cammi, R.; Pomelli, C.; Ochterski, J. W.; Martin, R. L.; Morokuma, K.; Zakrzewski, V. G.; Voth, G. A.; Salvador, P.; Dannenberg, J. J.; Dapprich, S.; Daniels, A. D.; Farkas, O.; Foresman, J. B.; Ortiz, J. V.; Cioslowski, J.; Fox, D. J. *Gaussian 09*, revision B.01; Gaussian, Inc.: Wallingford CT, 2010; see also <http://www.gaussian.com/>.
- (79) Lee, C.; Yang, W.; Parr, R. G. *Phys. Rev. B* **1988**, *37*, 785–789.
- (80) Becke, A. D. *J. Chem. Phys.* **1993**, *98*, 5648–5652.
- (81) Zhao, Y.; Truhlar, D. G. *Theor. Chem. Acc.* **2008**, *120*, 215–241.
- (82) Schreiner, E.; Nair, N. N.; Marx, D. *J. Am. Chem. Soc.* **2009**, *131*, 13668–13675.
- (83) Ardevol, A.; Rovira, C. *Angew. Chem.*, 2011, published online; DOI: 10.1002/anie.201104623.
- (84) Alfonso-Prieto, M.; Oberhofer, H.; Klein, M. L.; Rovira, C.; Blumberger, J. *J. Am. Chem. Soc.* **2011**, *133*, 4285–4298.
- (85) Ardevol, A.; Biarnes, X.; Planas, A.; Rovira, C. *J. Am. Chem. Soc.* **2010**, *132*, 16058–16065.
- (86) Petersen, L.; Ardevol, A.; Rovira, C.; Reilly, P. J. *J. Am. Chem. Soc.* **2010**, *132*, 8291–8300.
- (87) Schreiner, E.; Nair, N. N.; Marx, D. *J. Am. Chem. Soc.* **2008**, *130*, 2768–2770.
- (88) Laio, A.; Rodriguez-Fortea, A.; Gervasio, F. L.; Ceccarelli, M.; Parrinello, M. *J. Phys. Chem. B* **2005**, *109*, 6714–6721.
- (89) Dellago, C.; Bolhuis, P. G.; Csajka, F. S.; Chandler, D. *J. Chem. Phys.* **1998**, *108*, 1964–1977.
- (90) Park, J. M.; Laio, A.; Iannuzzi, M.; Parrinello, M. *J. Am. Chem. Soc.* **2006**, *128*, 11318–11319.
- (91) Henderson, R. *J. Mol. Biol.* **1970**, *54*, 341–354.
- (92) Robertus, J. D.; Kraut, J.; Alden, R. A.; Birktoft, J. *J. Biochemistry* **1972**, *11*, 4293–4303.
- (93) Kraut, J. *Annu. Rev. Biochem.* **1977**, *46*, 331–358.
- (94) Sharma, S.; Bandyopadhyay, P. *J. Mol. Model.* **2012**, *18*, 481–492.